Available online at www.sciencedirect.com
ScienceDirect
Continental Shelf Research 28 (2008) 137–158
CONTINENTAL SHELF RESEARCH
www.elsevier.com/locate/csr

A novel technique for detection of the toxic dinoflagellate, *Karenia brevis*, in the Gulf of Mexico from remotely sensed ocean color data

Jennifer P. Cannizzaro[a,*], Kendall L. Carder[a], F. Robert Chen[a], Cynthia A. Heil[b], Gabriel A. Vargo[a]

[a]*College of Marine Science, University of South Florida, St. Petersburg, FL 33701, USA*
[b]*Florida Fish and Wildlife Conservation Commission, Fish and Wildlife Research Institute, St. Petersburg, FL 33701, USA*

Received 22 May 2003; received in revised form 7 January 2004; accepted 15 April 2004
Available online 25 September 2007

Abstract

Karenia brevis, a toxic dinoflagellate that blooms regularly in the Gulf of Mexico, frequently causes widespread ecological and economic damage and can pose a serious threat to human health. A means for detecting blooms early and monitoring existing blooms that offers high spatial and temporal resolution is desired. Between 1999 and 2001, a large bio-optical data set consisting of spectral measurements of remote-sensing reflectance ($R_{rs}(\lambda)$), absorption ($a(\lambda)$), and backscattering ($b_b(\lambda)$) along with chlorophyll *a* concentrations and *K. brevis* cell counts was collected on the central west Florida shelf (WFS) as part of the Ecology and Oceanography of Harmful Algal Blooms (ECOHAB) and Hyperspectral Coastal Ocean Dynamics Experiment (HyCODE) programs. Reflectance model simulations indicate that absorption due to cellular pigmentation is not responsible for the factor of ~3–4 decrease observed in $R_{rs}(\lambda)$ for waters containing greater than 10^4 cells l^{-1} of *K. brevis*. Instead, particulate backscattering is responsible for this decreased reflectivity. Measured particulate backscattering coefficients were significantly lower when *K. brevis* concentrations exceeded 10^4 cells l^{-1} compared to values measured in high-chlorophyll (>1.5 mg m^{-3}), diatom-dominated waters containing fewer than 10^4 cells l^{-1} of *K. brevis*. A classification technique for detecting high-chlorophyll, low-backscattering *K. brevis* blooms is developed. In addition, a method for quantifying chlorophyll concentrations in positively flagged pixels using fluorescence line height (FLH) data obtained from the Moderate Resolution Imaging Spectroradiometer (MODIS) is introduced. Both techniques are successfully applied to Sea-viewing Wide Field-of-view Sensor (SeaWiFS) and MODIS data acquired in late August 2001 and validated using in situ *K. brevis* cell concentrations.

Keywords: Backscatter; Light absorption; Phytoplankton; Red tides; Remote sensing; USA; Florida; Gulf of Mexico; Geographic bounding coordinates: 28°N; 84.5°W; 26°N; 81°W

1. Introduction

Harmful algal blooms of the toxic, red tide dinoflagellate, *Karenia brevis* (formerly *Gymnodinium breve*), occur regularly in the Gulf of Mexico, typically in late summer and fall (Steidinger et al.,

*Corresponding author. Tel.: +1 727 553 3954; fax: +1 727 553 1189.
E-mail address: jpatch@marine.usf.edu (J.P. Cannizzaro).

0278-4343/$ - see front matter © 2007 Elsevier Ltd. All rights reserved.
doi:10.1016/j.csr.2004.04.007

1998). While blooms have been reported in coastal waters throughout the Gulf of Mexico and as far north as North Carolina (Tester et al., 1991), they occur most frequently along the west Florida shelf (WFS). *K. brevis* cells produce brevetoxins that accumulate in filter-feeding shellfish (i.e. oysters, clams, etc.) and when ingested by humans can cause Neurotoxic Shellfish Poisoning (Hemmert, 1975). Shellfish beds are ordered closed when *K. brevis* cell concentrations greater than 5000 cells l^{-1} are reported, making commercial shellfish industries extremely vulnerable to *K. brevis* blooms. Brevetoxins also cause bird, fish, and marine mammal mortalities (Landsberg and Steidinger, 1998) and can irritate human eyes and respiratory systems once they become airborne in sea spray (Hemmert, 1975; Asai et al., 1982). As a result, tourism industries have also incurred millions of dollars in lost revenue due to red tide events (Habas and Gilbert, 1974).

Based on historical data, *K. brevis* blooms typically initiate in nutrient-poor waters located between 18 and 74 km offshore (Steidinger, 1975; Steidinger and Haddad, 1981; Tester and Steidinger, 1997). While background concentrations of *K. brevis* (1–10^3 cells l^{-1}) are commonly found throughout the Gulf of Mexico (Steidinger, 1975), populations can increase to bloom proportions ($>10^4$ cells l^{-1}), causing fish kills ($\sim10^5$ cells l^{-1}) and water discoloration ($\sim10^6$ cells l^{-1}), provided that light and nutrient requirements are adequate (Steidinger et al., 1998; Walsh and Steidinger, 2001). Wind and currents then transport blooms inshore to coastal waters where they are often maintained along physical fronts and fueled by additional nutrient sources (Vargo et al., 2001). It is here where significant ecological and economic damage typically occurs as well as the greatest hazard to human health.

Current coastal management strategies employed by state agencies for detecting and monitoring red tide blooms in the Gulf of Mexico rely primarily on the collection of discrete samples from mainly nearshore waters after blooms have been transported inshore. These discrete samples (e.g. microscopic cell counts, toxin analyses, and chlorophyll concentrations) can be labor intensive and offer limited temporal and spatial resolution. As a result, data collected by coastal monitoring programs are susceptible to considerable bias and are often untimely in terms of providing early alerts to state and local officials.

To mitigate the human health risks and negative economic impacts associated with *K. brevis* blooms, an accurate system with high spatial and temporal resolution is required for identifying blooms early and for monitoring existing blooms. Since *K. brevis* blooms discolor oceanic surface waters (Carder and Steward, 1985; Vargo et al., 1987; Tester et al., 1998; Stumpf et al., 2003; Tomlinson et al., 2004), satellite-based ocean color sensors that provide daily coverage of kilometer-scale data may provide a robust tool for remotely detecting and monitoring blooms from space (Cullen et al., 1997; Schofield et al., 1999).

Ocean color sensors measure the amount of light reflected from the surface of the ocean at specific wavebands, from which the concentration of chlorophyll *a*, Chl, can be retrieved (Gordon et al., 1983; O'Reilly et al., 1998; Carder et al., 1999, 2004). However, since (1) all phytoplankton contain chlorophyll *a*, (2) other types of phytoplankton (e.g. diatoms) bloom regularly in the Gulf of Mexico (Lambert et al., 1999; Qian et al., 2003) and (3) chlorophyll estimates from space can be overestimated when algorithms that do not account for colored dissolved organic matter absorption (Carder et al., 1999; Hu et al., 2003) and bottom reflectance (Lee et al., 2001; Cannizzaro and Carder, 2006) are used, satellite-derived chlorophyll concentrations alone are not suitable for detecting *K. brevis* blooms from space. Instead, a robust technique capable of distinguishing *K. brevis* from other sources of true and apparent chlorophyll is required. Furthermore, since shellfish beds are ordered closed at a cell concentration level that is orders of magnitude lower than that found in monospecific blooms ($\sim10^6$ cells l^{-1}; Millie et al., 1997), discrimination of *K. brevis* in mixed populations is essential to alert coastal resource managers about potential blooms.

While algal quantity (i.e. Chl) can be derived relatively accurately from satellite-based ocean color data, identifying algal quality or the type of algae present is a more difficult task. Discriminating among algal groups requires systemic deviations in spectral absorption, $a(\lambda)$, and/or backscattering, $b_b(\lambda)$, coefficients. This is because the fraction of light entering the ocean that is reflected, or the remote-sensing reflectance, $R_{rs}(\lambda)$, is dominated by the ratio of $b_b(\lambda)$ to $a(\lambda)$ (Morel and Prieur, 1977). While certain types of phytoplankton (e.g. coccolithophores and *Trichodesmium* spp.) exhibit anomalously high backscattering that allow them to be

Table 1
ECOHAB (EH,EB) and HyCODE (HY) cruise data summary

Cruise	Dates	Surface discrete[a]	Surface underway[b]
EH0399	03/01/99–03/04/99	+	–
EH0799	07/05/99–07/08/99	+	–
EH0999	09/07/99–09/10/99	+	–
EH1199	11/06/99–11/08/99	+	–
EH0100	01/11/00–01/14/00	+	–
EH0300	03/01/00–03/04/00	+	–
EH0800	08/02/00–08/05/00	+	+
EH0900	09/06/00–09/08/00	–	+
EH1000	10/04/00–10/06/00	+	+
EH1100	11/07/00–11/10/00	+	+
EB0201	02/06/01–02/07/01	+	+
EH0401	04/03/01–04/06/01	+	+
EH0601	06/05/01–06/08/01	+	+
EH0701	06/30/01–07/03/01	+	+
EH0801	08/01/01–08/02/01	+	+
EH0901	08/28/01–08/31/01	+	+
EB0901	08/29/01–08/30/01	+	–
EB1001	10/01/01–10/02/01	+	–
HY1001	10/04/01–10/04/01	+	–

[a]Discrete measurements include *K. brevis* cell concentrations, HPLC pigments, fluorometric Chl, $a_p(\lambda)$, $a_d(\lambda)$, $a_g(\lambda)$, and $R_{rs}(\lambda)$.
[b]Underway measurements include salinity, b_b(488,676), and c(532).

identified from space (Balch et al., 1991; Subramaniam et al., 1999), *K. brevis* is a relatively weak backscatterer since it is large (20–40 μm) and exhibits a low index of refraction relative to seawater (1.05) (Mahoney, 2003).

Earlier bio-optical studies of *K. brevis* focused primarily on absorption properties (Millie et al., 1997; Lohrenz et al., 1999; Kirkpatrick et al., 2000), ignoring backscattering properties. This was most likely because the magnitude and spectral dependency of backscattering is typically much weaker than absorption (Morel and Prieur, 1977). Also, commercially available instrumentation for measuring backscattering had only recently become available (Maffione and Dana, 1997). Prior modeling efforts (Carder and Steward, 1985; Mahoney, 2003) and recent field measurements (Cannizzaro et al., 2004; Schofield et al., 2006), however, indicate that *K. brevis* blooms exhibit relatively low backscattering per unit chlorophyll.

The objective of this study is to develop techniques based on shipboard data to (1) classify *K. brevis* blooms and (2) quantify blooms (i.e. Chl) that can be applied to remotely sensed (e.g. satellite, aircraft, buoy, ship, etc.) ocean color data. A large, multi-year/multi-season, comprehensive database of Chl, absorption, backscattering, and remote-sensing reflectance data collected on the central WFS as part of the Ecology and Oceanography of Harmful Algal Blooms (ECOHAB) and Hyperspectral Coastal Ocean Dynamics Experiment (HyCODE) programs is used for this purpose. Total absorption and backscattering spectra are decomposed into the sum of their optically significant constituents (particulate, dissolved, and molecular). A chlorophyll-based, semi-analytical reflectance model is then used to determine whether absorption and/or backscattering is responsible for differences observed in remote-sensing reflectance spectra between *K. brevis* blooms ($>10^4$ cells l^{-1}) and non-*K. brevis* blooms ($<10^4$ cells l^{-1}).

2. Methods

Field data were collected on the WFS between March 1999 and October 2001 during 18 monthly survey cruises as part of the ECOHAB program and one HyCODE cruise (Table 1, Fig. 1). Discrete surface samples were collected with an 8-l Niskin bottle.

Samples for *K. brevis* enumeration were collected directly by siphoning 15 ml of water from the Niskin bottles into clean scintillation vials and were counted within 30 min of collection. Vials were gently inverted and then five replicates of 100–200 μl of sample were pipetted directly into glass well slides. Cells were counted live using a dissecting

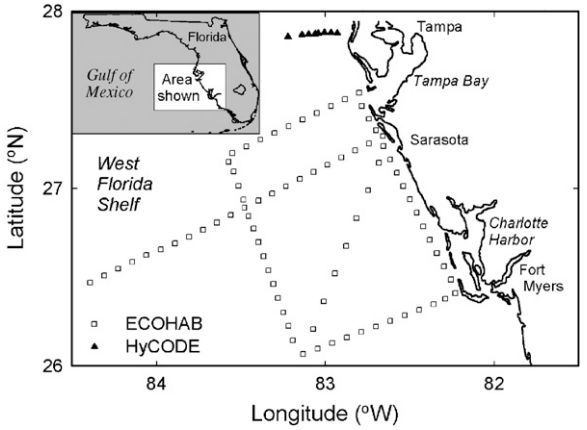

Fig. 1. Map of the west Florida shelf study area showing ECOHAB and HyCODE stations.

microscope at 40× magnification with *K. brevis* cells identified by morphological features and characteristic swimming motion. Average cell counts were calculated from the replicate samples.

Chorophylls *a*, *b* and *c* and carotenoid pigment concentrations were measured using high-performance liquid chromatography (HPLC) (Wright et al., 1991) by the research group of Dr. Gary Kirkpatrick (Mote Marine Laboratory, Sarasota, FL). Pigments were separated with a C-18 Hypersil reverse-phase column and identified using a photodiode array UV–vis detector (Shimadzu). Pigment absorbance spectra from standard microalgal cultures were used to identify and quantify the pigments.

Absorption spectra due to all particles (phytoplankton and detritus), $a_p(\lambda)$, and detritus, $a_d(\lambda)$, were determined using the quantitative filter technique (Yentsch, 1962; Kiefer and SooHoo, 1982) with a custom-made, 512-channel spectroradiometer (~350–850 nm). Pathlength elongation was corrected for using the β factor developed by Carder et al. (1999). Particulate absorption spectra with optical densities at 675 nm less than 0.04 were omitted to minimize errors due uncertainties in the β factor (Mitchell, 1990). Detrital absorption spectra were obtained by chemical separation using hot methanol (Kishino et al., 1985; Roesler et al., 1989). Phytoplankton absorption spectra, $a_{ph}(\lambda)$, were then calculated as

$$a_{ph}(\lambda) = a_p(\lambda) - a_d(\lambda). \quad (1)$$

Chlorophyll *a* and pheopigment concentrations were determined fluorometrically (Holm-Hansen and Riemann, 1978) on the methanol extracts.

A Perkin–Elmer Lambda 18 spectrophotometer equipped with 10 cm pathlength cells was used to measure gelbstoff absorption spectra, $a_g(\lambda)$. Gelbstoff is the dissolved (<0.2 μm) pool of colored compounds also commonly referred to as colored dissolved organic matter (CDOM). Gelbstoff absorption spectra were processed according the methods reported in Mueller and Fargion (2002).

Underway measurements of salinity, backscattering, and beam attenuation were measured with a CTD (Falmouth-Scientific Instruments), a Hydroscat-2 (HOBI Labs), and a C-Star transmissometer (WET Labs), respectively, during the 2000 and 2001 ECOHAB cruises. The instruments were mounted on a metal frame that was placed in a black-walled chamber (0.5 m^3). Seawater was pumped by the ship flow-through system from a depth of ~2 m through the chamber. Hydroscat-2 measurement, calibration, and data processing information are described in Maffione and Dana (1997). Backscattering coefficients at other wavelengths were calculated by fitting a spectral power function to the measured wavebands (488 and 676 nm) and then interpolating to the desired wavelength. Particulate backscattering coefficients, $b_{bp}(\lambda)$, were derived from total backscattering by subtracting the backscattering due to pure water (Morel, 1974). Particulate scattering at 532 nm, $b_p(532)$, was obtained by subtracting $a_p(532)$ and $a_g(532)$ from the beam attenuation coefficient at 532 nm, $c(532)$, once the attenuation of pure water was removed.

A custom-made, 512-channel spectroradiometer (~350–850 nm) equipped with a 10° field-of-view was used to measure remote-sensing reflectance spectra, $R_{rs}(\lambda)$. Data collection and processing information are described in Lee et al. (1996).

SeaWiFS data were processed using SeaDAS (version 4.3) software. Water-leaving radiances for visible wavebands were converted to $R_{rs}(\lambda)$ by dividing by the spectral extraterrestrial solar irradiances (Gordon and Wang, 1994). Interactive Data Language (IDL) software was then used to process the $R_{rs}(\lambda)$ data using the Carder et al. (1999) semi-analytical algorithm. MODIS Terra Collection 4 data were obtained from the NASA Goddard Distributed Active Archive Center (DAAC).

3. Theoretical considerations

Remote-sensing reflectance is defined as the ratio of water-leaving radiance to down welling irradiance, measured just above the sea surface.

For optically deep, vertically homogeneous water columns, $R_{rs}(\lambda)$ is dependent on the absorption and backscattering properties of seawater and the angular distribution of light within the ocean. Using radiative transfer theory, $R_{rs}(\lambda)$ can be expressed as

$$R_{rs}(\lambda) = \frac{t^2}{n^2}\frac{f}{Q(\lambda)}\frac{b_b(\lambda)}{a(\lambda)+b_b(\lambda)}. \quad (2)$$

(Lee et al., 1994) where t is the transmittance across the air–sea interface, n is the index of refraction of seawater, f is an empirical factor that is a function of the solar zenith angle, and $Q(\lambda)$ is the upwelling irradiance-to-radiance ratio.

By making approximations for these latter terms (Lee et al., 1998), $R_{rs}(\lambda)$ can be related to the subsurface remote-sensing reflectance, $r_{rs}(\lambda)$, as follows:

$$R_{rs}(\lambda) = \frac{0.5 r_{rs}(\lambda)}{(1-1.5 r_{rs}(\lambda))}. \quad (3)$$

Based on model simulations (Lee et al., 1999), $r_{rs}(\lambda)$ for optically deep waters is

$$r_{rs}(\lambda) = (0.084 + 0.17u)u, \quad (4)$$

where

$$u = \frac{b_b(\lambda)}{a(\lambda)+b_b(\lambda)} \quad (5)$$

The absorption coefficient can be examined more thoroughly by breaking it down into the sum of its components:

$$a(\lambda) = a_{ph}(\lambda) + a_d(\lambda) + a_g(\lambda) + a_w(\lambda), \quad (6)$$

where the subscripts ph, d, g, and w refer to phytoplankton, detritus, gelbstoff, and water, respectively. Similarly, the backscattering coefficient can be expanded as

$$b_b(\lambda) = b_{bp}(\lambda) + b_{bw}(\lambda), \quad (7)$$

where the subscripts p and w refer to total particles (phytoplankton and detritus) and water, respectively. Since $a_w(\lambda)$ and $b_{bw}(\lambda)$ are known (Morel, 1974), $R_{rs}(\lambda)$ can then be calculated from $a_{ph}(\lambda)$, $a_d(\lambda)$, $a_g(\lambda)$, and $b_{bp}(\lambda)$ (Eqs. (3)–(7)).

4. Shipboard remote-sensing reflectance data

Median remote-sensing reflectance spectra measured between 1999 and 2001 in waters containing fewer than 10^4 cells l^{-1} of *K. brevis* (Fig. 2A) are indicative of typical conditions on the WFS. Oligotrophic, offshore waters with chlorophyll concentrations less than 0.2 mg m^{-3} reflect blue light (~400–450 nm) strongly. Recalling that $R_{rs}(\lambda)$ is proportional to $b_b(\lambda)$ and inversely proportional to $a(\lambda)$ (Eq. (2)), blue reflectance values are relatively high in these waters because absorption dominates backscattering in this spectral region and the absolute magnitude of absorption is relatively low (Morel and Prieur, 1977).

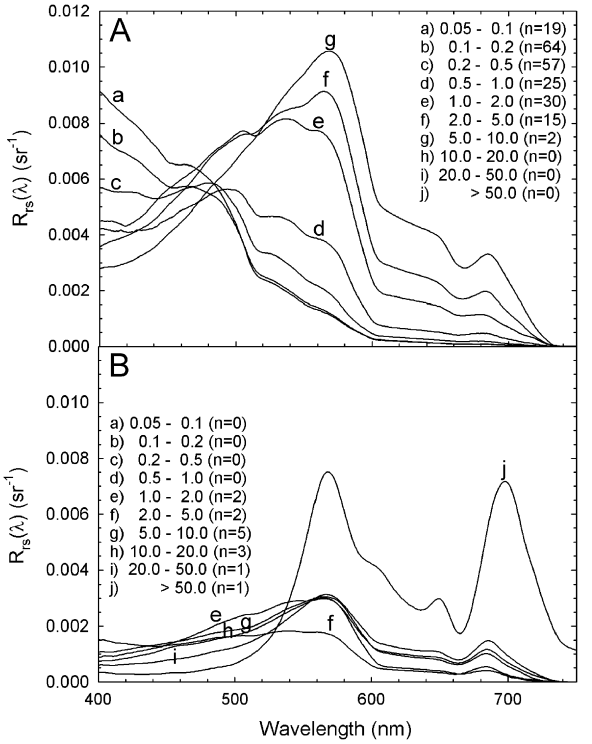

Fig. 2. Median remote-sensing reflectance spectra measured on the WFS between 1999 and 2001 for *K. brevis* cell concentrations (A) less than 10^4 cells l^{-1} and (B) greater than 10^4 cells l^{-1}, for various concentrations of chlorophyll (mg m^{-3}).

Transitioning from offshore to coastal waters, increases in absorption due to increased concentrations of chlorophyll and non-living material (e.g. detritus and gelbstoff) cause blue reflectance values to decrease. Meanwhile, reflectance values at green wavelengths (~500–600 nm) increase making waters visually appear green. This occurs because particulate backscattering increases while contributions by absorption to $R_{rs}(\lambda)$ are minimal in this spectral region (Bricaud et al., 1998). Peak reflectance values, in turn, shift from 400 to ~570 nm with increasing particle concentrations while transitioning from low-chlorophyll, offshore waters to high-chlorophyll, coastal waters.

In high-chlorophyll waters (~1–10 mg m^{-3}), remote-sensing reflectance values are ~3–4 times

lower in waters containing greater than 10^4 cells l^{-1} of *K. brevis* (Fig. 2B) compared to waters containing fewer than 10^4 cells l^{-1} of *K. brevis* for wavelengths less than 600 nm. This decrease in $R_{rs}(\lambda)$ observed in *K. brevis* blooms would cause the water to appear darker since the green reflectance peak at ~570 nm is less prominent. Indeed, when *K. brevis* cell concentrations exceeded 10^4 cells l^{-1}, instead of appearing green in color, the waters visually appeared olive green. Further increases in Chl beyond 10 mg m^{-3} are accompanied by further decreases in $R_{rs}(\lambda)$, causing the water to appear black in color. Although a red reflectance peak (~685–700 nm) due to chlorophyll *a* fluorescence becomes increasingly significant with increasing Chl (Fig. 2B), *K. brevis* blooms do not appear as red in color visually as they do radiometrically because the color receptors of the human eye are only slightly sensitive to this portion of the visible spectrum (Mobley, 1994).

5. Reflectance model

5.1. Model parameterization

To determine how differences in absorption and backscattering spectra influence $R_{rs}(\lambda)$ and in particular what causes reflectance values in *K. brevis* blooms ($>10^4$ cells l^{-1}) to be ~3–4 times lower than in non-*K. brevis* blooms ($<10^4$ cells l^{-1}), a sensitivity analysis was performed. Remote-sensing reflectance spectra were modeled using a chlorophyll-based, semi-analytical reflectance model developed by combining Eqs. (3)–(7). The model was parameterized using relationships determined below from shipboard data.

5.1.1. Phytoplankton absorption

Phytoplankton absorption spectra are composed of overlapping absorption spectra due to individual pigments that belong to three main groups: chlorophylls, carotenoids, and phycobiliproteins (Bidigare et al., 1989; Hoepffner and Sathyendranath, 1991). Two major absorption peaks at ~440 and 675 nm, mainly due to chlorophyll *a*, are typical of most $a_{ph}(\lambda)$ curves (Fig. 3A). Accessory pigments absorb light between ~450 and 550 nm, producing absorption shoulders and occasional peaks (Fig. 3A inset). Along with pigment variability, $a_{ph}(\lambda)$ are also influenced by pigment packaging (Nelson et al., 1993; Allali et al., 1997; Stuart et al., 1998). Essentially, increased cell size and intracellular pigment concentration causes self-shading, which leads to decreased absorption per unit chlorophyll, manifested as a flattening of absorption peaks (Morel and Bricaud, 1981).

The relationship between Chl and $a_{ph}(\lambda)$ can be expressed by a power function

$$a_{ph}(\lambda) = A(\lambda)\mathrm{Chl}^{B(\lambda)}, \tag{8}$$

where $A(\lambda)$ and $B(\lambda)$ are constants derived empirically from log-transformed data. Surface chlorophyll *a* concentrations observed on the WFS between 1999 and 2001 span more than two orders of magnitude, ranging from ~0.1 to 20 mg m^{-3} (Fig. 3B). Phytoplankton absorption coefficients at 443 nm, $a_{ph}(443)$, range from ~0.01 to 0.70 m^{-1} and are highly correlated with Chl ($r^2 = 0.98$, $n = 290$). Compared to a function derived by Bricaud et al. (1998) for a global dataset, the WFS exhibits higher phytoplankton absorption at 443 nm per unit chlorophyll. Increased concentrations of photosynthetic carotenoids relative to Chl and/or decreased pigment packaging on the WFS may explain this difference (Stuart et al., 1998). Both conditions are typical of highlight, subtropical oceanic waters such as the WFS.

Partitioning the dataset based on *K. brevis* cell concentrations; the following relationships were determined on log-transformed data

$$a_{ph}(443) = 0.057\mathrm{Chl}^{0.755} \quad \text{for} < 10^4 \text{ cells } l^{-1} \quad (r^2 = 0.95, n = 260), \tag{9a}$$

$$a_{ph}(443) = 0.051\mathrm{Chl}^{0.772} \quad \text{for} > 10^4 \text{ cells } l^{-1} \quad (r^2 = 0.93, n = 30). \tag{9b}$$

Using Student's *t*-test, the difference between the slope coefficients, $B(\lambda)$, derived for *K. brevis* populations less than and greater than 10^4 cells l^{-1} was insignificant ($\alpha = 0.05$) at 443 nm.

Values for $A(\lambda)$ and $B(\lambda)$ were determined every nanometer between 400 and 700 nm to parameterize the reflectance model (Fig. 4). *K. brevis* bloom and non-*K. brevis* bloom waters exhibit similar spectral shape coefficients, $A(\lambda)$, for wavelengths greater than ~500 nm (Fig. 4A), although $A(443)$ is 13% lower in *K. brevis* blooms. Since *K. brevis* cells are relatively large (20–40 μm) and low-light adapted (Shanley and Vargo, 1993), decreased phytoplankton absorption per unit Chl may be caused by increased pigment packaging and/or decreased concentrations of photoprotective carotenoids relative to Chl, respectively.

Slope coefficients derived for waters containing less than and greater than 10^4 cells l^{-1} of *K. brevis*

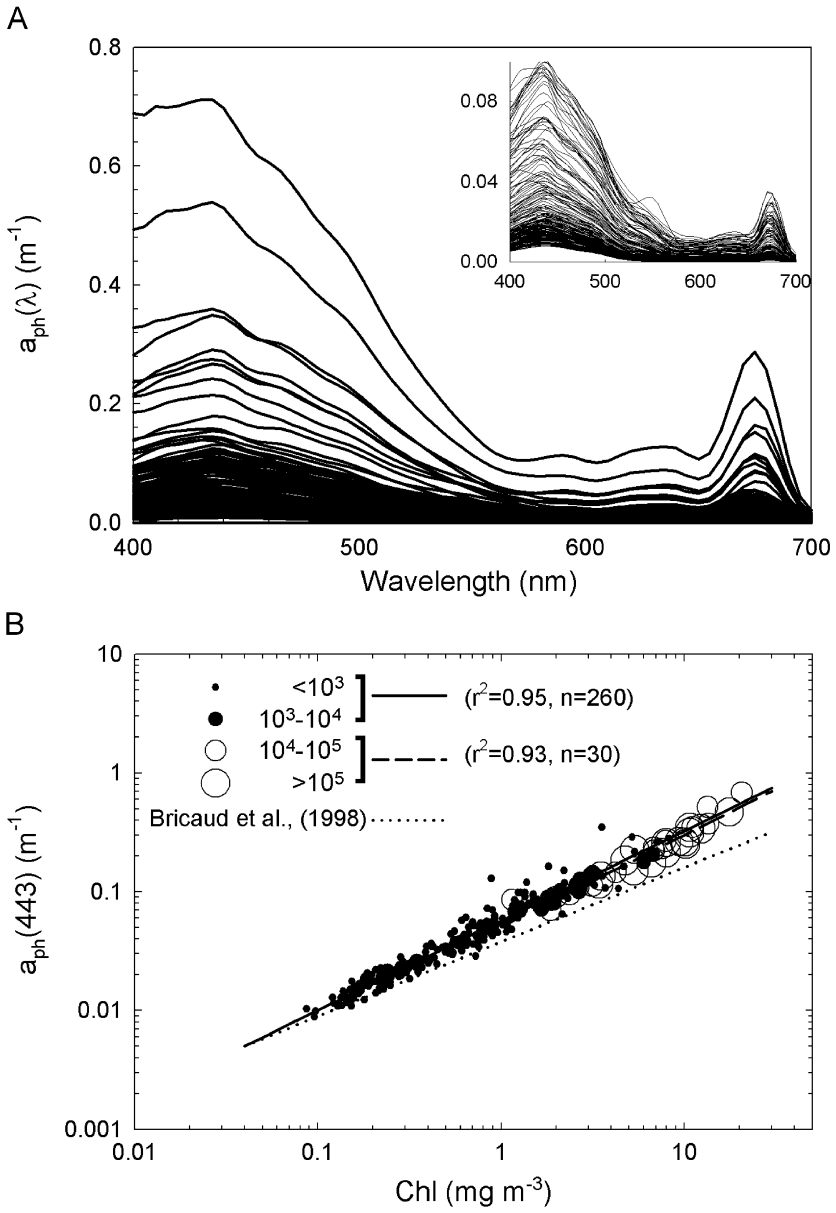

Fig. 3. (A) Surface phytoplankton absorption spectra measured on the WFS between 1999 and 2001. (B) Relationship between Chl and phytoplankton absorption at 443 nm. Symbol size increases with increasing *K. brevis* cell concentrations (cells l^{-1}). Regression lines for cell concentrations less than 10^4 cells l^{-1} (solid) and greater than 10^4 cells l^{-1} (dashed) were obtained by least-squares linear regression on log-transformed data. The relationship developed by Bricaud et al. (1998) for a global data set (dotted) is shown for comparison.

are similar for wavelengths less than 500 nm and greater than 590 nm (Fig. 4B). For wavelengths between 500 and 590 nm, *K. brevis* blooms exhibit lower slopes than non-*K. brevis* bloom waters. In fact, $B(\lambda)$ values derived for wavelengths between 520 and 575 nm were significantly different ($\alpha = 0.05$), perhaps due to increased concentrations of phycobiliproteins and/or decreased pigment packaging in non-*K. brevis* bloom waters. Slopes derived for wavelengths less than 520 nm and greater than 575 nm were not significantly different ($\alpha = 0.05$).

Coefficients of determination for wavelengths less than 500 nm are slightly lower in waters containing greater than 10^4 cells l^{-1} of *K. brevis* ($r^2 = \sim 0.93$, $n = 30$) compared to waters containing fewer than 10^4 cells l^{-1} of *K. brevis* ($r^2 = \sim 0.95$, $n = 260$) (Fig. 4C). Coefficients of determination are

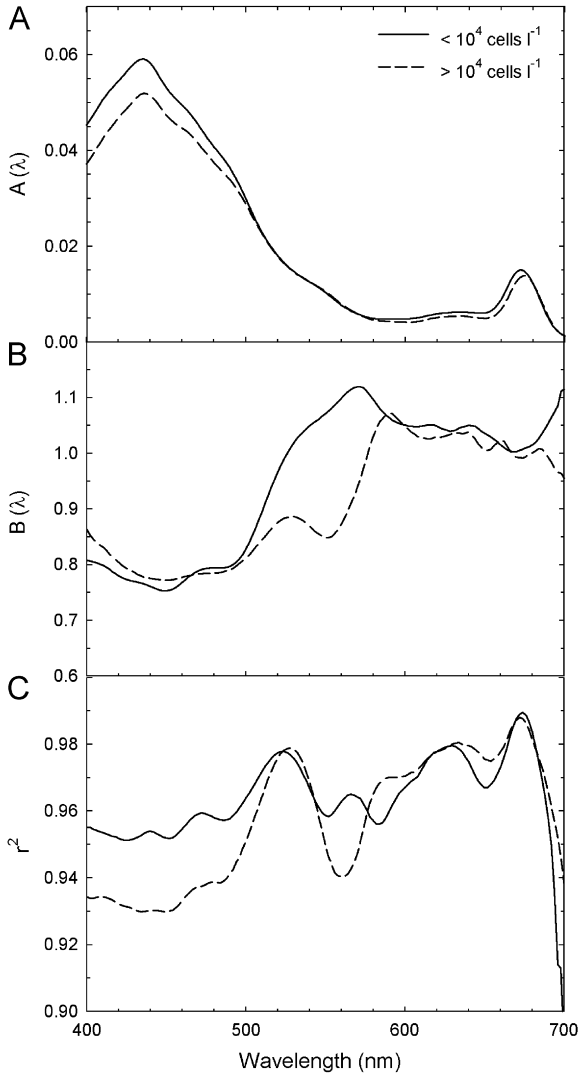

Fig. 4. Spectral values of the coefficients (A) $A(\lambda)$ and (B) $B(\lambda)$ obtained by fitting a power law function to log-transformed $a_{ph}(\lambda)$ versus Chl data, and (C) the coefficient of determination, r^2. Coefficients were determined in 1 nm increments from 400 to 700 nm for waters containing less than (solid) and greater than (dashed) 10^4 cells l^{-1} of *K. brevis*.

maximal for both groups at 675 nm because non-chlorophyll *a* pigments absorb light weakly at this wavelength. Since the total concentration of accessory pigments typically co-varies strongly with Chl in oceanic waters (Trees et al., 2000), the relationships between Chl and $a_{ph}(\lambda)$ for wavelengths between 490 and 550 nm also exhibit high coefficients of determination ($r^2 > 0.93$) even though chlorophyll *a* does not absorb light in this region.

5.1.2. Detrital absorption

Detrital absorption spectra exhibit exponentially decreasing absorption with increasing wavelength (Fig. 5A) (Yentsch, 1962; Roesler et al., 1989) and can be modeled as

$$a_d(\lambda) = a_d(\lambda_0)\exp(-S_d(\lambda - \lambda_0)), \quad (10)$$

where λ_0 is a reference wavelength and S_d is the spectral slope for detrital absorption. For waters containing relatively high concentrations of phycobiliproteins, residual absorption peaks are present between ~450 and 550 nm (Fig. 5A inset) since these pigments are non-methanol soluble. Modeled detrital absorption spectra for these stations were generated using Eq. (10) to eliminate these peaks and used instead of the measured spectra in Eq. (1) to derive $a_{ph}(\lambda)$.

Detrital absorption at 443 nm, $a_d(443)$, ranges from ~0.001 to 0.14 m^{-1} for surface stations measured on the WFS between 1999 and 2001 (Fig. 5B). $a_d(443)$ constitutes a small and variable fraction (~5–40%) of the total particulate absorption at 443 nm. This latter range is consistent with values reported for tropical to subpolar waters (Cleveland, 1995; Bricaud et al., 1998). Trends between Chl and $a_d(443)/a_p(443)$ were not observed (data not shown).

Since the sources and sinks of this non-living particulate pool of colored compounds are often independent of phytoplankton in coastal regions such as the WFS, a weaker positive correlation exists between Chl and $a_d(443)$ ($r^2 = 0.88$, $n = 290$) (Fig. 5B) compared to between Chl and $a_{ph}(443)$ (Fig. 3B). Partitioning the data set based on *K. brevis* concentrations, the following relationships were developed from log-transformed data:

$$a_d(443) = 0.014\mathrm{Chl}^{1.030} \text{ for } < 10^4 \text{ cells } l^{-1} \quad (r^2 = 0.78, n = 260), \quad (11a)$$

$$a_d(443) = 0.014\mathrm{Chl}^{0.581} \text{ for } > 10^4 \text{ cells } l^{-1} \quad (r^2 = 0.36, n = 30). \quad (11b)$$

Non-*K. brevis* bloom waters containing fewer than 10^4 cells l^{-1} exhibit a steeper slope compared to bloom waters containing greater than 10^4 cells l^{-1}. Differences between these slopes are significantly different ($\alpha = 0.05$), indicating that *K. brevis* blooms exhibit a paucity of detrital absorption on the WFS compared to similarly high-chlorophyll (> ~1 mg m^{-3}), non-*K. brevis* bloom waters.

Spectral slopes for detrital absorption generated between 400 and 650 nm vary from ~0.009 to

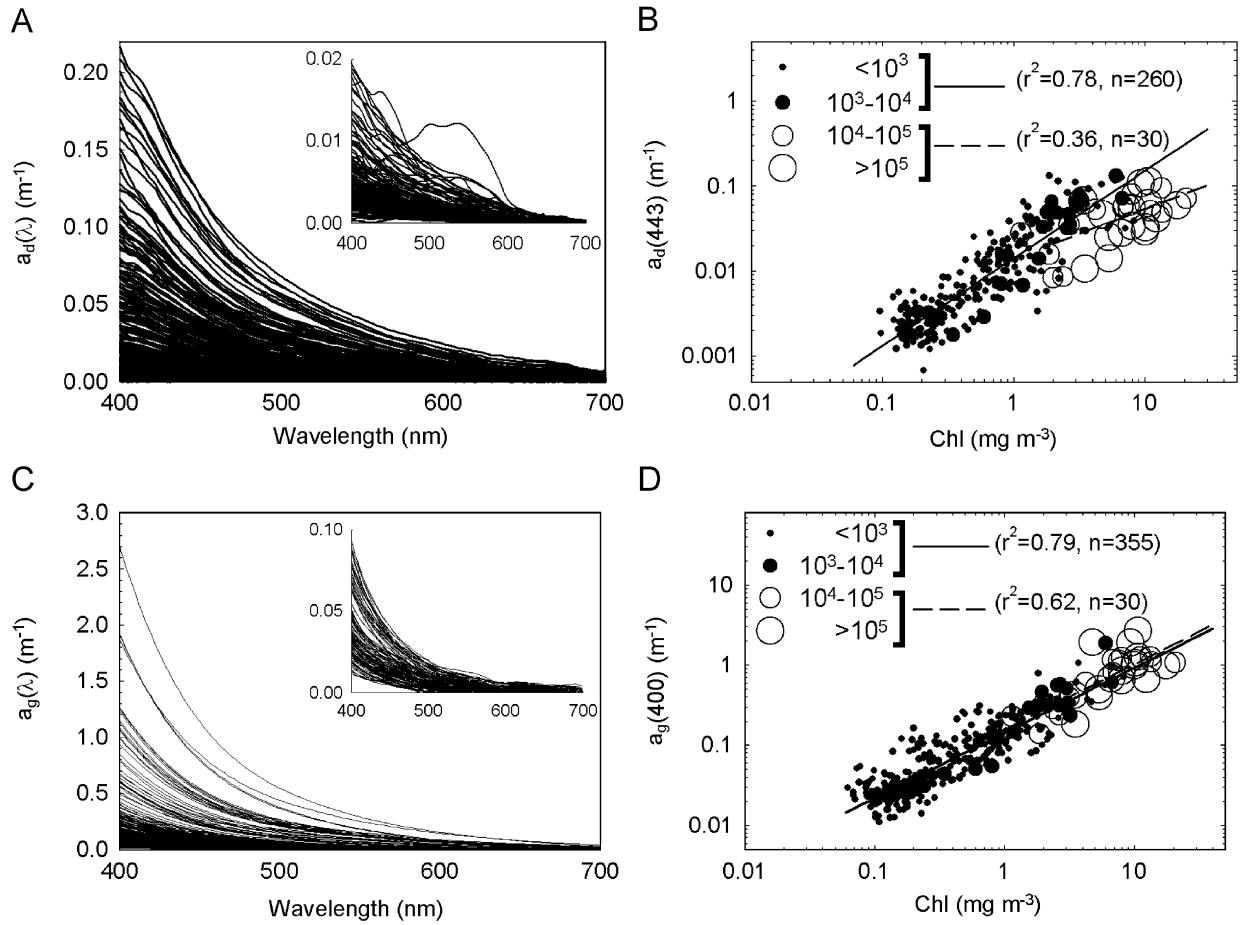

Fig. 5. Surface (A) detrital and (C) gelbstoff absorption spectra measured on the WFS between 1999 and 2001 and relationships between Chl and (B) detrital absorption at 443 nm and (D) gelbstoff absorption at 400 nm.Symbol size increases with increasing *K. brevis* cell concentrations (cells l^{-1}). Regression lines for cell concentrations less than 10^4 cells l^{-1} (solid) and greater than 10^4 cells l^{-1} (dashed) were obtained by least-squares linear regression on log-transformed data.

$0.015\,nm^{-1}$ (data not shown) and are consistent with values reported for other oceanic regions (Roesler et al., 1989; Bricaud et al., 1998). Average S_d values observed on the WFS between 1999 and 2001 for three Chl ranges (0.1–1, 1–10, and 10–100 mg m^{-3}) are 0.011, 0.011, and $0.012\,nm^{-1}$, respectively. Since detrital spectral slopes do not co-vary with Chl ($r^2 = 0.00$, $n = 290$), the mean detrital spectral slope, $0.012 \pm 0.001\,nm^{-1}$, is used together with the relationships in Eq. (11) to generate $a_d(\lambda)$ (Eq. (10)) for the reflectance model.

5.1.3. Gelbstoff absorption

Gelbstoff absorption spectra exhibit spectral features similar to the detrital pool of colored compounds, absorbing blue light strongly and showing decreased absorption with increased wavelength (Fig. 5C). Thus, $a_g(\lambda)$ can be modeled as

$$a_g(\lambda) = a_g(\lambda_0)\exp(-S_g(\lambda - \lambda_0)), \quad (12)$$

where S_g is the spectral slope for gelbstoff absorption. Since gelbstoff absorption is roughly two times greater at 400 nm than at 443 nm, a reference wavelength of 400 nm was chosen since it offers greater signal-to-noise when a 10 cm spectrophotometric cell is used for measuring $a_g(\lambda)$.

Gelbstoff absorption at 400 nm, $a_g(400)$, ranges from ~0.01 to $2.7\,m^{-1}$ for surface stations measured on the WFS from 1999 to 2001 (Fig. 5D). This range is approximately an order of magnitude higher than that observed for $a_d(400)$ (Fig. 5A). $a_g(400)$ is positively correlated with Chl ($r^2 = 0.92$, $n = 385$) (Fig. 5D). Partitioning the data set based on *K. brevis* cell concentrations, the following relationships were

developed from log-transformed data:

$$a_g(400) = 0.142\text{Chl}^{0.814} \text{ for} < 10^4 \text{ cells l}^{-1} \quad (r^2 = 0.79, n = 355), \tag{13a}$$

$$a_g(400) = 0.156\text{Chl}^{0.818} \text{ for} > 10^4 \text{ cells l}^{-1} \quad (r^2 = 0.62, n = 30). \tag{13b}$$

The difference between the slopes for these two groups is insignificant ($\alpha = 0.05$), indicating that gelbstoff absorption, unlike detrital absorption, is not unique in *K. brevis* blooms.

Spectral slopes for gelbstoff absorption calculated between 350 and 450 nm ranges from ~0.014 to 0.025 nm^{-1} and are generally higher than the slopes measured for detrital absorption. Data for wavelengths greater than 450 nm were not considered due to signal-to-noise problems. The variability of S_g is high for chlorophyll concentrations less than 1 mg m^{-3} with an average slope of 0.020 ± 0.002 nm^{-1}. Waters with chlorophyll concentrations greater than 1 mg m^{-3} exhibit a mean spectral slope of 0.019 ± 0.001 nm^{-1} that is slightly lower than that observed for lower chlorophyll concentrations and shows decreased variability. Similar S_g ranges and variability have been reported for other oceanic waters (Carder et al., 1989; Blough et al., 1993; Nelson and Guarda, 1995; Vodacek and Blough, 1997). Since S_g is only weakly correlated with Chl ($r^2 = 0.09$, $n = 385$) (data not shown), the mean gelbstoff spectral slope, 0.019 ± 0.002 nm^{-1}, is used together with the relationships in Eq. (13) to calculate $a_g(\lambda)$ (Eq. (12)) for the reflectance model.

5.1.4. Particulate backscattering

Particulate backscattering spectra can be fit to the form

$$b_{bp}(\lambda) = b_{bp}(\lambda_0)\left(\frac{\lambda_0}{\lambda}\right)^{\gamma}, \tag{14}$$

where γ is the Angstrom exponent that describes the spectral shape. A reference wavelength of 550 nm was chosen to parameterize the reflectance model since changes in $R_{rs}(\lambda)$ at this wavelength are primarily due to changes in backscattering. At 550 nm, water absorption is constant (Pope and Fry, 1997) and non-water absorption is relatively low (Figs. 3A, 5A, and C).

Particulate backscattering at 550 nm, $b_{bp}(550)$, ranges from ~0.001 to 0.08 m^{-1} for surface stations measured on the WFS in 2000 and 2001 (Fig. 6A). A positive correlation exists between Chl and $b_{bp}(550)$ ($r^2 = 0.85$, $n = 194$). For low chlorophyll concentrations (<~0.5 mg m^{-3}), $b_{bp}(550)$ is strongly correlated with Chl, while for higher chlorophyll concentrations a weaker correlation is observed.

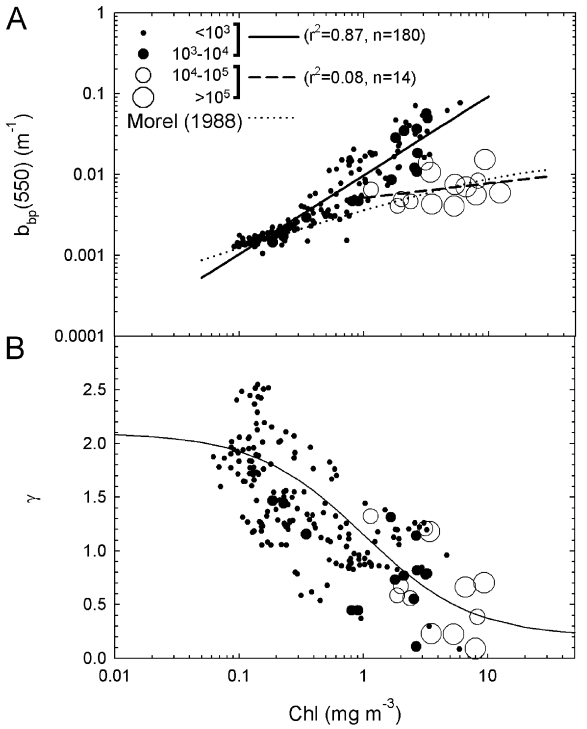

Fig. 6. (A) Relationship between Chl and particulate backscattering at 550 nm for surface data collected on the WFS in 2000 and 2001. Symbol size increases with increasing *K. brevis* cell concentrations (cells l^{-1}). Regression lines for cell concentrations less than 10^4 cells l^{-1} (solid) and greater than 10^4 cells l^{-1} (dashed) were obtained by least-squares linear regression on log-transformed data. An empirical relationship determined by Morel (1988) for modeled Case 1 data (dotted) is shown for comparison. (B) Relationship between Chl and the $b_{bp}(\lambda)$ spectral shape parameter, γ. An empirical function (solid) developed for all *K. brevis* cell concentrations is shown.

Partitioning the data based on *K. brevis* cell concentrations, the following relationships were developed from log-transformed data:

$$b_{bp}(550) = 0.0098\text{Chl}^{0.977} \text{ for} < 10^4 \text{ cells l}^{-1} \quad (r^2 = 0.87, n = 180), \tag{15a}$$

$$b_{bp}(550) = 0.0051\text{Chl}^{0.180} \text{ for} > 10^4 \text{ cells l}^{-1} \quad (r^2 = 0.08, n = 14). \tag{15b}$$

Statistical analyses confirm that the slope derived in *K. brevis* blooms is significantly lower ($\alpha = 0.05$) than the slope derived in non-*K. brevis* bloom

waters. The expression obtained for *K. brevis* bloom waters (Eq. (15b)) is very similar to a relationship generated for modeled Case 1 data (Morel, 1988). Case 1 waters have detrital and gelbstoff absorption coefficients that co-vary with phytoplankton, while such a correlation does not exist in Case 2 waters (Preisendorfer, 1961).

Unlike the spectral slopes for detrital and gelbstoff absorption, the Angstrom exponent for particulate backscattering is strongly correlated with Chl ($r^2 = 0.53$, $n = 194$) (Fig. 6B). A negative correlation is observed between γ and Chl, with no significant differences observed between waters containing less than or greater than 10^4 cells l^{-1} of *K. brevis*. Thus, the following best-fit relationship, modified from Lee and Carder (2000),

$$\gamma = 0.1 + \frac{1.9}{(1 + \mathrm{Chl})}, \quad (16)$$

was developed for this data set. Eq. (16) ensures that γ approaches asymptotes for low and high chlorophyll concentrations that are consistent with modeled data (Gordon et al., 1988). Together with the relationships in Eq. (15), $b_{bp}(\lambda)$ can now be derived from Chl for the reflectance model.

Comparing the Chl and $b_{bp}(550)$ data collected on the WFS in 2000 and 2001 to the Morel (1988) Case 1 expression (Fig. 6A), the WFS can be separated into three bio-optically unique provinces:

1. Data collected from oligotrophic waters, typically west of the 30 m isobath (i.e. away from terrigenous influences), exhibit low chlorophyll concentrations ($< \sim 0.2\,\mathrm{mg\,m^{-3}}$), low $b_{bp}(550)$ coefficients, and *K. brevis* concentrations less than 10^4 cells l^{-1}. These data generally overlay the Case 1 line. Pigment concentrations provided by HPLC indicate that these waters were dominated by prochlorophytes and cyanophytes since they exhibited relatively high concentrations of the marker pigments divinyl-chlorophyll

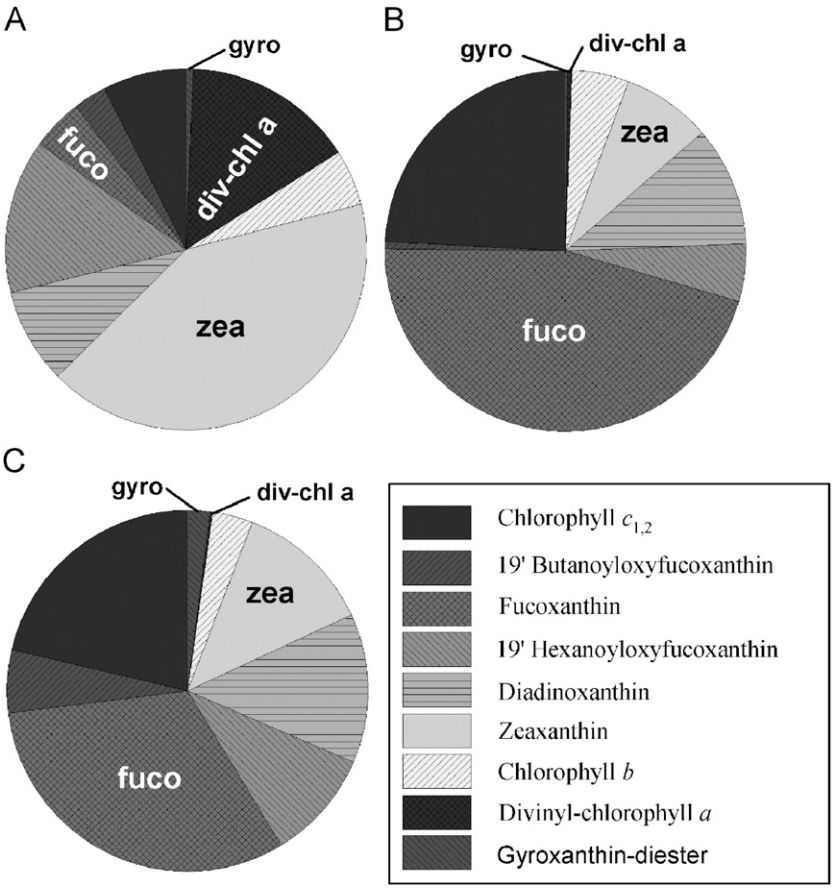

Fig. 7. Relative composition of the main accessory pigments for (A) low-chlorophyll ($<0.2\,\mathrm{mg\,m^{-3}}$), non-*K. brevis* bloom waters, (B) high-chlorophyll ($>1.0\,\mathrm{mg\,m^{-3}}$), non-*K. brevis* bloom waters, and (C) high-chlorophyll ($>1.0\,\mathrm{mg\,m^{-3}}$), *K. brevis* bloom waters.

a and zeaxanthin, respectively (Fig. 7A) (Wright et al., 1991).

2. Shallow, coastal waters, containing fewer than 10^4 cells l^{-1} of *K. brevis*, typically located just outside of Tampa Bay and Charlotte Harbor, exhibit high chlorophyll concentrations ($>\sim$1.0 mg m^{-3}) and high $b_{bp}(550)$ coefficients. These data deviate significantly from the Case 1 relationship and are instead consistent with Case 2 waters containing large concentrations of high-backscattering particles. Relatively high concentrations of the marker pigment fucoxanthin (Fig. 7B) along with microscopic analyses indicate that diatoms dominated these waters.
3. Regions containing *K. brevis* cell concentrations greater than 10^4 cells l^{-1} also have high chlorophyll concentrations ($>\sim$1.0 mg m^{-3}), but they exhibited lower $b_{bp}(550)$ coefficients compared to diatom-dominated, coastal waters. Data from these regions generally overlay the Case 1 line and contained the *K. brevis* diagnostic marker pigment, gyroxanthin-diester (Fig. 7C) (Millie et al., 1995).

5.2. Model application

Relationships derived between Chl and $a_{ph}(\lambda)$, $a_d(\lambda)$, $a_g(\lambda)$, and $b_{bp}(\lambda)$ for waters containing fewer than 10^4 cells l^{-1} of *K. brevis* were used to create a library of non-*K. brevis* bloom $R_{rs}(\lambda)$ spectra for a wide range of chlorophyll concentrations (0.05–20 mg m^{-3}). Relationships generated from waters containing greater than 10^4 cells l^{-1} of *K. brevis* were then substituted one at a time into the model to determine which parameter(s) is (are) responsible for the 3- to 4- fold decrease in $R_{rs}(\lambda)$ observed in *K. brevis* blooms (Fig. 2) with two exceptions:

1. The influence of $a_g(\lambda)$ on $R_{rs}(\lambda)$ was not examined since the difference between Chl and $a_g(400)$ was insignificant for waters containing less than and greater than 10^4 cells l^{-1} of *K. brevis* (Fig. 5D).
2. Secondly, the relationship generated between Chl and $b_{bp}(550)$ in *K. brevis* bloom waters was replaced by the modeled Case 1 expression (Morel, 1988) to provide reasonable particulate backscattering coefficients for low chlorophyll concentrations (Fig. 6A).

Modeled $R_{rs}(\lambda)$ values generated for waters containing less than and greater than 10^4 cells l^{-1} of *K. brevis* were then compared by examining $R_{rs}(\lambda)$ at 443, 488 and 551 nm as a function of Chl (Fig. 8).

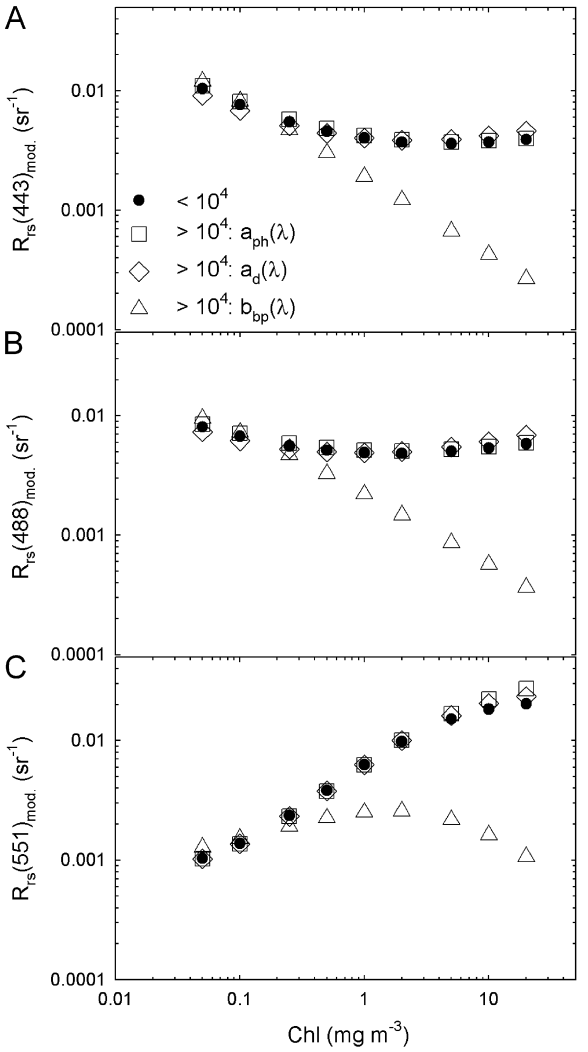

Fig. 8. Relationships between modeled Chl and remote-sensing reflectance coefficients at (A) 443 nm, (B) 488 nm, and (C) 551 nm. Modeled $R_{rs}(\lambda)$ values were derived from a semi-analytical reflectance model parameterized using relationships between Chl and both absorption and backscattering coefficients developed in this study. Non-*K. brevis* bloom $R_{rs}(\lambda)$ values (filled circles) were derived using relationships developed between Chl and $a_{ph}(\lambda)$, $a_d(\lambda)$, $a_g(\lambda)$, and $b_{bp}(\lambda)$ from data with *K. brevis* concentrations less than 10^4 cells l^{-1}. Relationships between Chl and $a_{ph}(\lambda)$ (Eq. (9b); unfilled squares), Chl and $a_d(\lambda)$ (Eq. (11b); unfilled diamonds), and Chl and $b_{bp}(\lambda)$ (Morel, 1988; unfilled triangles) developed from data with *K. brevis* concentrations greater than 10^4 cells l^{-1} were substituted one at a time into the model.

Substituting the $a_{ph}(\lambda)$ parameters, $A(\lambda)$ and $B(\lambda)$, derived for *K. brevis* bloom waters (Figs. 4A, B) into the model, reflectance values similar to non-*K. brevis* bloom values were observed at 443 and 490 nm (Figs. 8A, B). Reflectance values at 555 nm,

though, were slightly higher than non-*K. brevis* bloom values for higher chlorophyll concentrations (Fig. 8C). An increase in reflectance at 555 nm occurs because the slope coefficient at this wavelength was significantly lower in bloom waters compared to non-*K. brevis* bloom waters (Fig. 4B). Increases in $R_{rs}(\lambda)$ were also observed when the relationship derived for *K. brevis* blooms between Chl and $a_d(\lambda)$ was substituted into the reflectance model. However, since $a_d(\lambda)$ generally constitutes a very small portion of the total absorption spectra, only minor deviations in $R_{rs}(\lambda)$ were observed.

Together, the results of these model simulations indicate that the lower chlorophyll-specific phytoplankton absorption, $a^*_{ph}(\lambda)(=a_{ph}(\lambda)/\mathrm{Chl})$, and chlorophyll-specific detrital absorption, $a^*_d(\lambda)(=a_d(\lambda)/\mathrm{Chl})$, values observed in *K. brevis* blooms (Figs. 4 and 5) result in slightly higher $R_{rs}(\lambda)$ values compared to those observed in non-*K.brevis* blooms. Thus, the 3- to 4- fold decrease in $R_{rs}(\lambda)$ observed in *K. brevis* bloom waters (Fig. 2B) cannot be explained by deviations in absorption. Furthermore, since these deviations are relatively minor, they cannot be used as a basis for detecting *K. brevis* blooms from space using remotely sensed ocean color data.

Substituting the Morel (1988) Case 1 relationship between Chl and $b_{bp}(550)$ into the reflectance model as a surrogate for the relationship developed for *K. brevis* blooms (Fig. 6A), decreases in $R_{rs}(\lambda)$ at 443, 488, and 551 nm by a factor of 2–10 were observed relative to non-*K. brevis* bloom values for chlorophyll concentrations from 1 to 10 mg m^{-3}, respectively (Fig. 8). Thus, the 3- to 4-fold decrease in $R_{rs}(\lambda)$ observed in waters containing greater than 10^4 cells l^{-1} of *K. brevis* compared to those containing fewer than 10^4 cells l^{-1} of *K. brevis* can be attributed to decreases in particulate backscattering per unit chlorophyll.

6. Algorithms for classifying and quantifying *K. brevis* blooms from space

6.1. Classification algorithm

Based on the differences observed between Chl and $b_{bp}(550)$ (Fig. 6A) and the effects of particulate backscattering on $R_{rs}(\lambda)$ (Fig. 8), a technique is developed to discriminate high-chlorophyll ($>\sim$1 mg m^{-3}), high-*K. brevis* ($>10^4$ cells l^{-1}) waters from high-chlorophyll, low-*K. brevis* ($<10^4$ cells l^{-1}) waters. However, since Chl and $b_{bp}(550)$ cannot be measured directly by satellite-based ocean color sensors, a semi-analytical algorithm (Carder et al. 1999) developed for MODIS data is used to derive these values given $R_{rs}(\lambda)$ at 412, 443, 488, and 551 nm. Assuming that reflectance values at SeaWiFS wavebands (412, 443, 490, and 555 nm) are not significantly different from MODIS wavebands, the classification technique developed here may be applied to both MODIS and SeaWiFS data.

Particulate backscattering at 550 nm can be calculated from $R_{rs}(551)$ using the expression derived by Carder et al. (1999): $b_{bp}(550) = 2.058\ R_{rs}(551) - 0.00182$. The root mean square error (rms) determined between measured and modeled log-transformed $b_{bp}(550)$ data is 0.14 ($r^2 = 0.90$, $n = 120$) (Fig. 9A).

For Case 2 environments such as the WFS, chlorophyll concentrations determined semi-analytically have an advantage over empirical spectral ratio algorithms (Gordon et al., 1983; O'Reilly et al., 1998) since corrections for gelbstoff and detrital absorption that often do not co-vary with Chl are made. Gelbstoff and detritus can absorb enough light at blue wavelengths to increase empirically retrieved chlorophyll concentrations by as much as a factor of two (Hu et al., 2003). The semi-analytical algorithm separates the effects of phytoplankton absorption from gelbstoff and detrital absorption based on spectral differences at 412 and 443 nm (Figs. 3A, 5A, and C). The rms error determined on log-transformed data between measured Chl and modeled Chl determined semi-analytically using global parameters is 0.19 ($r^2 = 0.95$, $n = 214$) (Fig. 9B).

Calculating $b_{bp}(550)$ from $R_{rs}(551)$, and plotting these values against the semi-analytically derived chlorophyll concentrations, a diagram (Fig. 9c) was generated based entirely on shipboard $R_{rs}(\lambda)$ data to show how satellite-based ocean color data can be used to classify populations of *K. brevis* greater than 10^4 cells l^{-1} from space. Note that the separation between clusters of observations representing *K. brevis* bloom and non-*K. brevis* bloom waters is even more distinct than was observed for the in situ measurements (Fig. 6A). This is probably due to the fact that $b_{bp}(550)$ is underestimated in *K. brevis* blooms (Fig. 9A) when derive from $R_{rs}(551)$ alone (Carder et al., 1999). While improved backscattering retrievals in absorption-rich waters (e.g. *K. brevis* blooms) can be obtained using algorithms/techniques that utilize wavebands longer than $\sim$600 nm (e.g. Lee et al., 1999; IOCCG, 2006), using such algorithms will decrease the separation between *K. brevis* and non-*K. brevis* bloom data in Fig. 9C making it more difficult to accurately classify blooms from Chl and backscattering data.

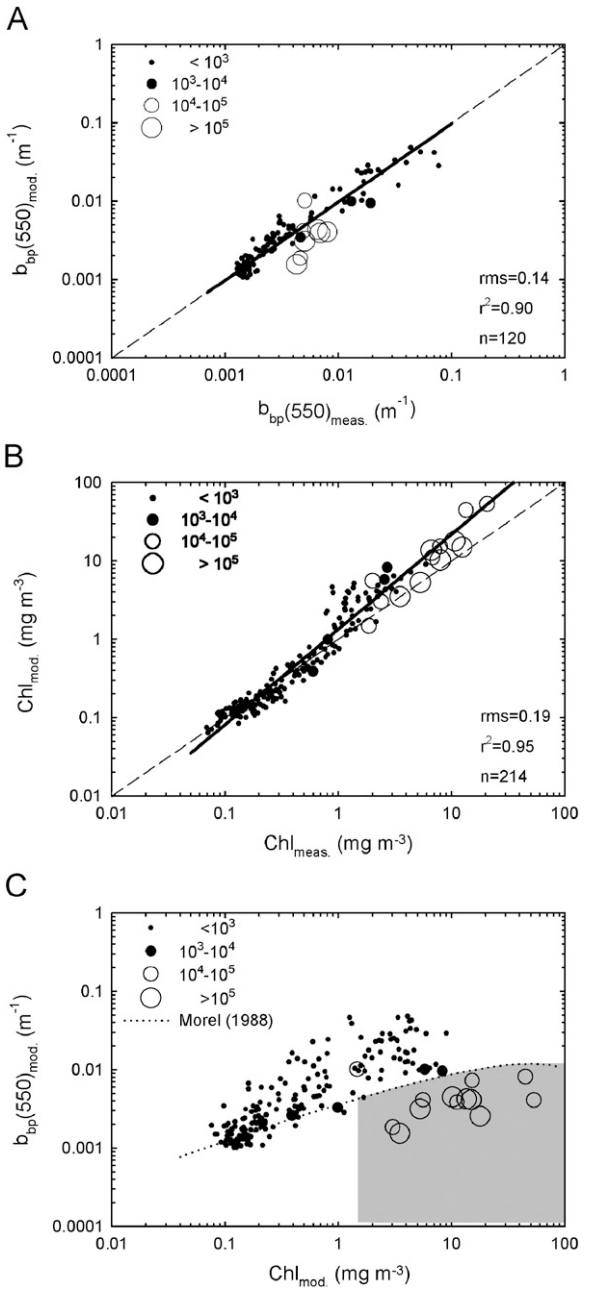

Fig. 9. Measured versus modeled (A) $b_{bp}(550)$ and (B) Chl from shipboard data collected on the WFS between 1999 and 2001. Modeled values were derived from $R_{rs}(\lambda)$ using the Carder et al. (1999) semi-analytical algorithm (global parameterization). Symbol size increases with increasing *K. brevis* cell concentrations (cells l^{-1}). Shown are best-fit regression lines (solid) obtained by least-squares linear regression on log-transformed data and one-to-one lines (dashed). (C) The relationship between modeled $b_{bp}(550)$ and modeled Chl data. The shaded area represents regions with Chl $>1.5\,mg\,m^{-3}$ and $b_{bp}(550)$ less than the Morel (1988) Case 1 relationship.

The data in Fig. 9C indicate that all observations with

1. Chlorophyll concentrations greater than $1.5\,mg\,m^{-3}$ and
2. $b_{bp}(550)$ values less than the Morel (1988) relationship.

contain greater than 10^4 cells l^{-1} of *K. brevis*. Only one observation with 14,000 cells l^{-1} (i.e. near detection limit) of *K. brevis* is not discriminated by this approach, and no false positive classifications are observed. As a result, these two conditions shall serve as the initial criteria for classifying *K. brevis* from space.

From Fall 2001 to Spring 2002, the central WFS experienced a major *K. brevis* bloom. The bloom first appeared in surface waters north of Charlotte Harbor in late August 2001, concentrated just north and west of a low salinity (~32.5 psu), estuarine plume dominated by diatoms. Three weeks of weak but steady northerly winds may have upwelled the bloom from a deeper offshore initiation source. Surface cell counts as high as 7.5×10^6 cells l^{-1} with chlorophyll concentrations $\sim 130\,mg\,m^{-3}$ were observed during an ECOHAB cruise along with salinities greater than 36 psu and particulate backscattering per unit chlorophyll values as low as $0.0006\,m^2\,(mg\,Chl)^{-1}$.

A SeaWiFS image acquired on 30 August 2001 shows a thin (~6 km) filament of high-chlorophyll water stretching ~65 km from just north of Charlotte Harbor offshore in a southerly direction (Fig. 10A). A smaller region of high chlorophyll concentrations ($>10\,mg\,m^{-3}$) is also observed outside of Tampa Bay. Deriving Chl and $b_{bp}(550)$ using the Carder et al. (1999) semi-analytical algorithm and then classifying the data based on the criteria defined previously, Fig. 10B shows that only regions with *K. brevis* concentrations greater than 10^4 cells l^{-1} are positively identified as *K. brevis* using this classification technique. Note that the high-chlorophyll waters observed outside of Tampa Bay containing fewer than 10^3 cells l^{-1} of *K. brevis* are not positively classified. These waters were instead dominated by the diatom *Rhizoselenia sp.* according to microscopic analyses.

6.2. Quantification algorithm

Quantifying *K. brevis* blooms accurately is important for estimating the contribution of *K. brevis* to

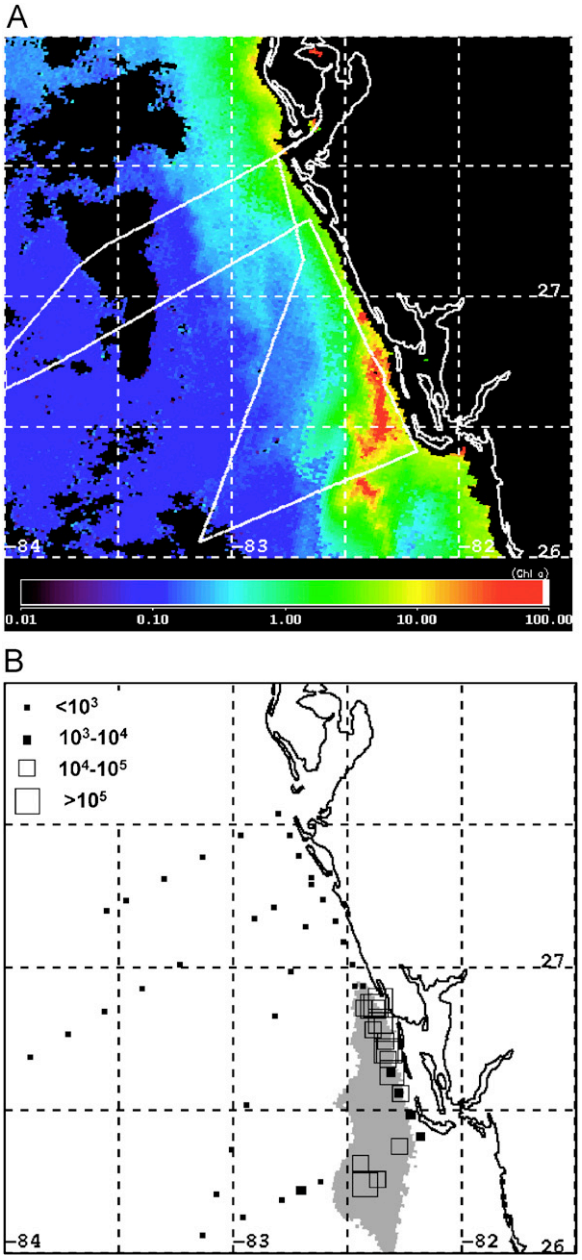

Fig. 10. (A) Chlorophyll concentrations (mg m^{-3}) derived using the Carder et al. (1999) semi-analytical algorithm (global parameterization) from SeaWiFS data of the WFS acquired on 30 August 2001. (B) Same image classified, whereby the shaded area represents regions with chlorophyll concentrations greater than 1.5 mg m^{-3} and $b_{bp}(550)$ values less than the Morel (1988) Case 1 relationship. Shipboard *K. brevis* cell concentrations (cells l^{-1}) measured 28–31 August 2001 are superimposed on top of the classified image. Symbol size increases with increasing *K. brevis* cell concentrations (cells l^{-1}).

annual water column production on the WFS (e.g. Vargo et al., 1987). Since most remote-sensing algorithms for deriving Chl (Gordon et al., 1983; O'Reilly et al., 1998; Carder et al., 1999) rely on $R_{rs}(\lambda)$ values at or below 490 nm, current space-based retrievals of accurate chlorophyll concentrations for extreme algal blooms (>100 mg m^{-3}) may oftentimes be inaccurate due to signal-to-noise errors at these wavelengths (Fig. 2B). This problem is only exacerbated in *K. brevis* blooms as decreased particulate backscattering per unit chlorophyll (Fig. 6A) leads to even lower $R_{rs}(\lambda)$ values compared to non-*K. brevis* bloom waters with similar chlorophyll concentrations (Figs. 2 and 8). Also, since the water-leaving radiance at 750 nm can no longer be considered negligible for use in atmospheric correction for extreme blooms (Siegel et al., 2000), low and even negative retrievals of $R_{rs}(\lambda)$ can occur at wavelengths below 490 nm due to over-correction of aerosol radiance (Hu et al., 2000), leading to Chl retrieval inaccuracies.

An alternative approach to standard algorithms is to quantify Chl in extreme blooms based on fluorescence since $R_{rs}(685)$ increases with Chl due to chlorophyll fluorescence (Fig. 2). While it is well understood that fluorescence efficiency is quite variable (Kiefer, 1973), if a firm relationship can be developed between Chl and the height of the reflectance peak, then perhaps more accurate chlorophyll concentrations can be obtained using this method compared to standard approaches.

Unlike SeaWiFS, MODIS contains wavebands designed to quantify this chlorophyll fluorescence peak. The MODIS fluorescence line height (FLH) data product is defined as

$$\mathrm{FLH} = \mathrm{nL_w}(\lambda_{14}) - \left[\mathrm{nL_w}(\lambda_{13}) - \frac{(\mathrm{nL_w}(\lambda_{13}) - \mathrm{nL_w}(\lambda_{15}))}{(\lambda_{15} - \lambda_{13})} \times (\lambda_{14} - \lambda_{13})\right], \quad (17)$$

where $\mathrm{nL_w}(\lambda)$ is the water-leaving radiance normalized so that the sun is at zenith and the numerical subscripts refer to the MODIS band number ($13 = 667$, $14 = 678$, and $15 = 748$ nm) (Esaias et al., 1998). Essentially, FLH is the height of the fluorescence contribution at 678 nm above a point directly below on a baseline to be found if no fluorescence was present. Note that the center fluorescence band could not be located at the nominal chlorophyll fluorescence peak wavelength at 685 nm because of an atmospheric oxygen absorption line, and so the 678 nm waveband was used on MODIS as a replacement.

Since shipboard measurements of $nL_w(\lambda)$ were not collected, they were derived by multiplying $R_{rs}(\lambda)$ by the extraterrestrial solar irradiance according to Gordon and Wang (1994). The relationship between Chl and FLH is shown in Fig. 11A. This diagram exhibits two separate trend lines: (1) a low slope for non-*K. brevis* bloom waters and (2) a higher slope for *K. brevis* blooms. The relationship generated for *K. brevis* blooms ($Chl = 143.0*FLH^{1.66}$, $r^2 = 0.85$, $n = 14$) is quite linear in log-log coordinates for chlorophyll concentrations greater than $\sim 1.5\,mg\,m^{-3}$, even up to concentrations as high as $130\,mg\,m^{-3}$. Thus, to the extent that *K. brevis* blooms can be identified using satellite-based ocean color data (e.g. Fig. 10B), chlorophyll concentrations may be estimated from MODIS FLH data (Fig. 11B).

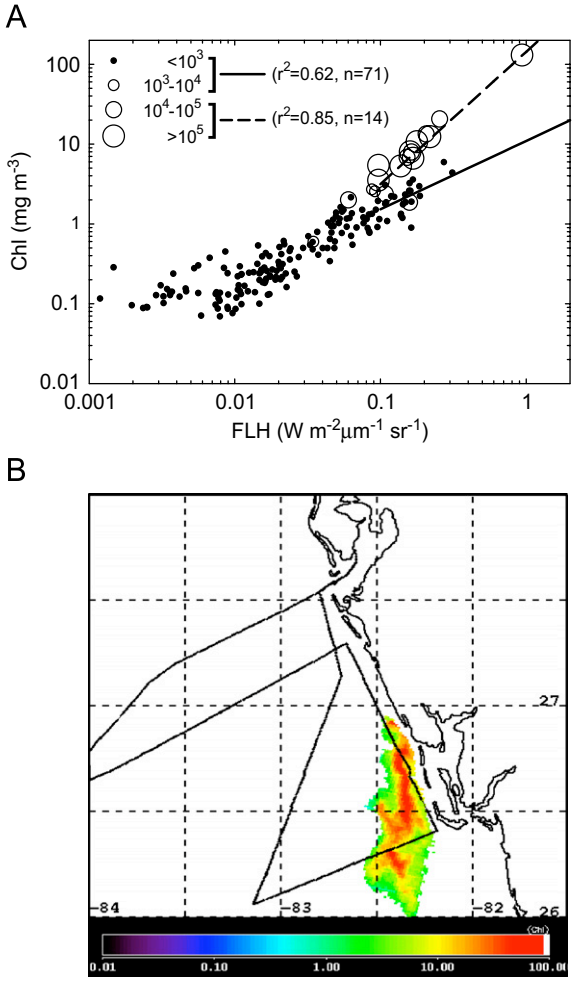

Fig. 11. (A) Surface in situ chlorophyll concentrations versus FLH data derived from shipboard $R_{rs}(\lambda)$ data. Symbol size increases with increasing *K. brevis* cell concentrations (cells l^{-1}). Regression lines for cell concentrations less than 10^4 cells l^{-1} (solid) and greater than 10^4 cells l^{-1} (dashed) were obtained by least-squares linear regression on log-transformed data. Only data with FLH's greater than $0.1\,W\,m^{-2}\,\mu m^{-1}\,sr^{-1}$, equivalent to Chl $\sim 1\,mg\,m^{-3}$, were regressed. (B) MODIS FLH data of the WFS acquired on 30 August 2001 converted to Chl ($mg\,m^{-3}$) using the relationship derived for cell concentrations greater than 10^4 cells l^{-1}. Only the region positively flagged for *K. brevis* is quantified.

7. Discussion

Shipboard remote-sensing reflectance values measured on the WFS between 1999 and 2001 were ~3–4 times lower on average in *K. brevis* blooms ($>10^4$ cells l^{-1}) compared to in non-*K. brevis* bloom waters ($<10^4$ cells l^{-1}). Model simulations indicate that this decrease in $R_{rs}(\lambda)$ cannot be attributed to deviations in absorption. These results refute the common perception that phytoplankton absorption (i.e. pigmentation) is responsible for the discoloration associated with *K. brevis* blooms. This is consistent with a previous study, which concluded that accurately identifying individual algal groups (i.e. diatoms, dinoflagellates, etc.) from space based on pigmentation is highly unlikely due to overlapping pigment absorption spectra and pigment packaging (Garver et al., 1994).

Indeed, classifying *K. brevis* blooms based solely on differences in $a_{ph}(\lambda)$ would be difficult for the following reasons. The main accessory pigments belonging to *K. brevis* (fucoxanthin, 19′acylofucoxanthins, and chlorophylls $c_{1,2}$ and c_3) co-occur in other algal groups (e.g. prymnesiophytes and chrysophytes). These groups are often present within natural mixed populations of *K. brevis* ($<10^6$ cells l^{-1}). Furthermore, the only pigment unique to *K. brevis*, gyroxanthin-diester, typically comprises less than 5% of the total pigment concentration and absorbs light in the same spectral region as the other carotenoids (Millie et al., 1995).

While natural populations of *K. brevis* have been discriminated successfully using a method based on in situ hyperspectral particulate absorption data (Kirkpatrick et al., 2000), this technique is not amenable to satellite-based ocean color data. Currently operating ocean color sensors (e.g. SeaWIFS and MODIS) are not hyperspectral and instead measure water-leaving radiances at fewer than eight visible wavebands. Also, extracting particulate absorption spectra from non-hyperspectral $R_{rs}(\lambda)$ is inherently difficult due to overlap with other optical constituents (Lee et al., 2001).

Particulate backscattering coefficients at 550 nm in waters containing greater than 10^4 cells l^{-1} of *K. brevis* were ~2.5–20 times lower for chlorophyll concentrations between ~1.5 and 20 mg m^{-3}, respectively, compared to waters containing fewer than 10^4 cells l^{-1} of *K. brevis*. Model simulations indicate that this decrease in $b_{bp}(\lambda)$ can explain the 3- to 4- fold decrease in $R_{rs}(\lambda)$ observed in *K. brevis* blooms. Thus, a technique was developed based on the relationship between Chl and $b_{bp}(550)$ to identify natural mixed populations of *K. brevis* from space at concentration levels one and two orders of magnitude lower than that which causes fish kills and water discoloration, respectively. The application of this classification technique to SeaWiFS data was considered successful since high-chlorophyll (>1.5 mg m^{-3}), low-backscattering *K. brevis* blooms were discriminated from high-chlorophyll, high-backscattering non-*K. brevis* blooms, which instead were dominated by diatoms.

7.1. Algorithm considerations

The techniques developed in this study for classifying and quantifying *K. brevis* blooms from space have several advantages over methods that rely solely on chlorophyll concentrations derived using standard empirical algorithms (Tester et al., 1998; Stumpf et al., 2003; Tomlinson et al., 2004). The relationship between Chl and $b_{bp}(550)$ is used to discriminate high-chlorophyll (>1.5 mg m^{-3}) waters containing less than and greater than 10^4 cells l^{-1} of *K. brevis*. Overestimations of Chl caused by high ratios of $a_g(\lambda)$ to $a_{ph}(\lambda)$, a common problem for standard empirical algorithms (Hu et al., 2003), are minimized by using a semi-analytical algorithm (Carder et al., 1999). Shallow water regions that exhibit reflectance signals contaminated by light reflected from the bottom will not be mistakenly flagged as *K. brevis* blooms. Although elevated $R_{rs}(551)$ values caused by bottom reflectance will lead to overestimations in Chl (Lee et al., 2001; Cannizzaro and Carder, 2006), particulate backscattering values derived from $R_{rs}(551)$ will also be erroneously high, preventing these regions from mistakenly being flagged as *K. brevis* blooms. Lastly, signal-to-noise errors that adversely affect empirically derived Chl estimates in extreme *K. brevis* blooms (>100 mg Chl m^{-3}) are eliminated when MODIS FLH data are used to quantify Chl.

Chlorophyll concentrations on the WFS typically increase when moving from offshore to near shore waters due to increased nutrient availability from terrigenous sources (e.g. riverine input and bottom resuspension). Increased absorption due to gelbstoff and increased backscattering due to detrital particles typically accompany this increase in chlorophyll. Model simulations indicate that false positive flagging of *K. brevis* blooms may occur if increases in Chl are accompanied by increases in gelbstoff absorption without similar increases in backscattering. A decrease in reflectance due to increased gelbstoff absorption, in this situation, would not be offset by an increase in reflectance if backscattering were relatively low. Subsequently, low $R_{rs}(551)$ values would lead to erroneously low backscattering values, which in turn would lead to false positive flagging for *K. brevis* bloom. One possible solution to this problem would be to use MODIS FLH data to discriminate between positively flagged regions containing *K. brevis* from false positively flagged high-gelbstoff absorption, low-backscattering regions since gelbstoff does not fluoresce at 678 nm (Hu et al., 2005).

While false positive flagging may occur when ratios of $a_g(\lambda)$ to $b_{bp}(\lambda)$ are anomalously high, false negative flagging may occur due to subpixel variability. Since dense algal blooms exhibit spatial patchiness (Franks, 1997) and may not occupy entire SeaWiFS or MODIS pixels (~1 km^2), extremely low reflectance values exhibited by spatially small *K. brevis* blooms may be overwhelmed by higher reflectance values from surrounding background populations of phytoplankton. Misclassifications may also occur if *K. brevis* blooms spatially co-exist with high-backscattering *Trichodesmium* blooms (Subramaniam et al., 1999; Walsh and Steidinger, 2001).

7.2. Why K. brevis bloom backscattering is low

To understand why backscattering is relatively low in *K. brevis* blooms, the major factors responsible for controlling backscattering in oceanic waters (i.e. particle size and composition) must be considered. While neither of these factors was measured directly during this study, inferences can be made regarding the nature of the particles present based on measurements of the backscattering ratio, $b_{bp}(\lambda)/b_p(\lambda)$ (e.g. Boss et al., 2004).

The backscattering ratio is the proportion of light scattered by particles in the backward direction, where $b_p(\lambda)$ is the scattering coefficient due to particles in all directions. Theoretical models

indicate that backscattering ratios decrease (increase) in response to

(1) decreases (increases) in the fraction of submicron particles (Ulloa et al., 1994) and
(2) decreases (increases) in the refractive index of particles (Twardowski et al., 2001).

Indices of refraction are strongly related to particle composition. Phytoplankton exhibit low indices of refraction (1.02–1.07, relative to water) (e.g. Carder et al., 1972) due to high water content and inorganic particles (e.g. minerals) exhibit high indices of refraction (1.14–1.26) (Lide, 1997).

Since in situ backscattering ratios measured on the WFS in 2000 and 2001 (~0.6–2.3%; data not shown) are significantly greater than ratios measured for pure phytoplankton (typically $<0.1\%$) (Bricaud et al., 1983; Ahn et al., 1992), only a small fraction of the particulate backscattering measured during this study can be attributed to living algal cells. Indeed, *K. brevis* is an ineffective backscatterer due to its large size (20–40 μm) and relatively low index of refraction (~1.05) (Mahoney, 2003). Instead, the primary source of particulate backscattering in oceanic waters is particles less than 1 μm (Morel and Ahn, 1991; Stramski and Kiefer, 1991). Thus, natural populations of phytoplankton on the WFS must contain significant concentrations of submicron particles in order to account for the high backscattering ratios observed during this study.

Backscattering ratios measured in high-chlorophyll ($>1.5\,mg\,m^{-3}$), *K. brevis* bloom waters ($<1.0\%$) are lower than ratios measured in high-chlorophyll, non-*K. brevis* bloom waters ($>1.0\%$). This indicates that the submicron particle composition differs between *K. brevis* bloom and non-*K. brevis* bloom waters, perhaps explaining the differences observed in backscattering (Fig. 6A). Similar backscattering ratios were observed during a *K. brevis* diel vertical migration experiment on the WFS in October 2001(Kerfoot et al., 2004).

The lower backscattering ratios measured in waters containing greater than $10^4\,cells\,l^{-1}$ of *K. brevis* indicate that *K. brevis* blooms must contain a paucity of submicron particles and/or particle assemblages with a lower bulk index of refraction compared to non-*K. brevis* bloom waters (Ulloa et al., 1994; Twardowski et al., 2001). Such conditions may explain the low backscattering observed in *K. brevis* blooms and could possibly arise from (1) reduced grazing pressure due to cellular toxicity and (2) the inability of *K. brevis* to out compete diatoms and succeed in high-backscattering, detritus-rich coastal environments.

Evidence that a paucity of detritus may have been associated with *K. brevis* blooms includes shipboard measurements of detrital absorption coefficients. If a positive correlation exists between detrital absorption and detrital concentration, then observations of decreased detrital absorption (Fig. 5B) indicate that *K. brevis* blooms may have had relatively low detrital concentrations. Reduced grazing pressure may partially be responsible for generating this paucity of detritus. Lower pheopigment-to-chlorophyll ratios measured in *K. brevis* blooms (0.10 ± 0.04, $n=26$) compared to those measured in high-chlorophyll ($>1.5\,mg\,m^{-3}$), non-*K. brevis* bloom waters (0.23 ± 0.10, $n=24$) indicate that zooplankton grazing pressure may have been lower in *K. brevis* blooms (Shuman and Lorenzen, 1975). Decreased pheopigment-to-chlorophyll ratios cannot be attributed to fast phytoplankton growth that outpaces grazing since *K. brevis* cells exhibit relatively slow growth rates, doubling only once every 3–5 days (Steidinger et al., 1998).

While relationships between *K. brevis* and zooplankton are complex, previous studies have demonstrated that grazing pressure declines in both natural populations and cultures of *K. brevis* possibly due to cellular toxicity (reviewed by Turner and Tester, 1997). Reduced concentrations of detrital substrates due to decreased grazing pressure would cause microbial populations to decline, perhaps leading to further reductions in detritus due to decreased microbial decomposition.

Not only may cellular toxicity reduce the concentration of submicron particles found in *K. brevis* blooms causing backscattering to decrease, differences in particle composition may exist between *K. brevis* bloom and non-bloom waters due to the environment inhabited by this organism. In general, fast-growing phytoplankton groups with high nutrient uptake efficiencies (e.g. diatoms) tend to dominate algal populations in high-nutrient waters (Smayda, 1997). High-nutrient coastal waters on the WFS typically contain large concentrations of terrigenous material derived from riverine outflow and sediment resuspension. This material is composed largely of inorganic particles with high indices of refraction, causing coastal waters to exhibit high backscatter coefficients.

Since *K. brevis* cells grow relatively slowly, they cannot out compete these faster growing phytoplankton groups and therefore occupy an ecological niche devoid of allochthonous sources of high-backscattering particles (i.e. Case 1 waters). High-salinity values ($>\sim$35 psu) observed in waters containing the highest concentrations of *K. brevis* for each bloom measured during this study reinforce the notion that blooms were not directly associated with low-salinity ($<\sim$35 psu), estuarine waters from Tampa Bay or Charlotte Harbor. Indeed, *K. brevis* has evolved numerous physiological and behavioral strategies (cellular toxicity, vertical migration, mixotrophic tendency, photoadaptation, etc.) (Steidinger et al., 1998) that allow it to succeed in low-backscattering, nutrient-poor environments, perhaps permitting its detection from space.

8. Summary

K. brevis blooms are optically unique from a remote sensing standpoint not due to the cells themselves, but due to the environment inhabited by the cells. A paucity of high-backscattering submicron particles caused by reduced grazing pressure due to cellular toxicity and decreased concentrations of terrestrial-derived inorganic material may be responsible for the low backscattering per unit chlorophyll values observed in *K. brevis* blooms on the WFS relative to high-chlorophyll ($>$ 1.5 mg m^{-3}), diatom-dominated coastal waters. Classification of *K. brevis* blooms based on this anomalously low backscattering may be possible using optical sensors capable of directly measuring Chl and $b_{bp}(550)$ or deriving these values from measurements of $R_{rs}(\lambda)$. Such sensors may be mounted on a variety of remote (satellite and aircraft) and in situ (moorings and ships) platforms in order to detect and monitor blooms on a variety of spatial and temporal scales. Quantification of extreme bloom events ($>$100 mg m^{-3}) may be improved using FLH data since a strong correlation was observed between FLH and Chl in *K. brevis* bloom waters. Upon future validation, the classification and quantification techniques developed in this study may be implemented into current and future monitoring programs as well as ecological models to complement existing remote and in situ technologies. Together, these techniques may allow coastal managers to better mitigate the harmful effects of *K. brevis* blooms on the WFS and throughout the Gulf of Mexico.

Acknowledgments

The authors wish to thank David English, Dan Otis, and Hari Warrior for assistance in data collection and processing and Dr. Gary Kirkpatrick, Brad Pederson, and Barb Berg (Mote Marine Laboratory) for processing the HPLC data. Financial support was provided by NASA (NAS5-31716) and ONR (N00014-97-1-0006 and N00014-96-1-5013) funding.

References

Ahn, Y., Bricaud, A., Morel, A., 1992. Light backscattering efficiency and related properties of some phytoplankters. Deep Sea Research 39, 1835–1855.

Allali, K., Bricaud, A., Claustre, H., 1997. Spatial variations in the chlorophyll-specific absorption coefficient of phytoplankton and photosynthetically active pigments in the equatorial Pacific. Journal of Geophysical Research 102, 12,413–12,423.

Asai, S., Krzanowski, J.J., Anderson, W.H., Martin, D.F., Polson, J.B., Lockey, R.F., Bukantz, S.C., Szentivanyi, A., 1982. Effects of the toxin of red tide, *Ptychodiscus brevis*, on canine tracheal smooth muscle: a possible new asthma-triggering mechanism. The Journal of Allergy and Clinical Immunology 69, 418–428.

Balch, W.M., Holligan, P.M., Ackleson, S.G., Voss, K.J., 1991. Biological and optical properties of mesoscale coccolithophore blooms in the Gulf of Maine. Limnology and Oceanography 36, 629–643.

Bidigare, R.R., Morrow, J.H., Kiefer, D.A., 1989. Derivative analysis of spectral absorption by photosynthetic pigments in the western Sargasso Sea. Journal of Marine Research 47, 323–341.

Blough, N.V., Zafiriou, O.C., Bonilla, J., 1993. Optical absorption spectra of waters from the Orinoco River outflow: terrestrial input of colored organic matter to the Caribbean. Journal of Geophysical Research 98, 2271–2278.

Boss, E., Pegau, W.S., Lee, M., Twardowski, M., Shybanov, E., Korotaev, G., Baratange, F., 2004. Particulate backscattering ratio at LEO 15 and its use to study particle compostion and distribution. Journal of Geophysical Research 109, C01014.

Bricaud, A., Morel, A., Prieur, L., 1983. Optical efficiency factors of some phytoplankters. Limnology and Oceanography 28, 816–832.

Bricaud, A., Morel, A., Babin, M., Allali, K., Claustre, H., 1998. Variations of light absorption by suspended particles with chlorophyll *a* concentration in oceanic (case 1) waters: analysis and implications for bio-optical models. Journal of Geophysical Research 103, 31,033–31,044.

Cannizzaro, J.P., Carder, K.L., 2006. Estimating chlorophyll *a* concentrations from remote-sensing reflectance in optically shallow waters. Remote Sensing of Environment 101, 13–24.

Cannizzaro, J.P., Carder, K.L., Chen, F.R., Walsh, J.J., Lee, Z.P., Heil, C., 2004. A novel optical classification technique for detection of red tides in the Gulf of Mexico: application to the 2001–2002 bloom event. In: Steidinger, K.A., Landsberg, J.H., Tomas, C.R., Vargo, G.A. (Eds.), Harmful Algae 2002. Florida Fish and Wildlife Conservation Commission, Florida

Institute of Oceanography, and Intergovernmental Oceanographic Commission of UNESCO, St. Petersburg, Florida, USA, pp. 282–284.

Carder, K.L., Steward, R.G., 1985. A remote-sensing reflectance model of a red-tide dinoflagellate off west Florida. Limnology and Oceanography 30, 286–298.

Carder, K.L., Tomlinson, R.D., Beardsley Jr., G.F., 1972. A technique for the estimation of indices of refraction of marine phytoplanktoners. Limnology and Oceanography 17, 833–839.

Carder, K.L., Steward, R.G., Harvey, G.R., Ortner, R.B., 1989. Marine humic and fulvic acids: their effects on remote sensing of ocean chlorophyll. Limnology and Oceanography 34, 68–81.

Carder, K.L., Chen, F.R., Lee, Z.P., Hawes, S.K., Kamykowski, D., 1999. Semi-analytic moderate-resolution imaging spectrometer algorithms for chlorophyll a and absorption with bio-optical domains based on nitrate-depletion temperatures. Journal of Geophysical Research 104, 5403–5422.

Carder, K.L., Chen, F.R., Cannizzaro, J.P., Campbell, J.W., Mitchell, B.G., 2004. Performance of MODIS semi-analytic ocean color algorithm for chlorophyll-*a*. Advances in Space Research 33, 1152–1159.

Cleveland, J.S., 1995. Regional models for phytoplankton absorption as a function of chlorophyll a concentration. Journal of Geophysical Research 100, 13,333–13,344.

Cullen, J.J., Ciotti, A.M., Davis, R.F., Lewis, M.R., 1997. Optical detection and assessment of algal blooms. Limnology and Oceanography 42, 1223–1239.

Esaias, W., Abbott, M., Barton, I., Brown, O.B., Campbell, J.W., Carder, K.L., Clark, D.K., Evans, R.H., Hoge, F.E., Gordon, H.R., Balch, W.M., Letelier, R., Minnett, P.J., 1998. An overview of MODIS capabilities for ocean science observations. IEEE Transactiions on Geoscience and Remote Sensing 36, 1250–1265.

Franks, P.J.S., 1997. Spatial patterns in dense algal blooms. Limnology and Oceanography 42, 1297–1305.

Garver, S.A., Siegel, D.A., Mitchell, B.G., 1994. Variability in near surface particulate absorption spectra: what can a satellite ocean color imager see? Limnology and Oceanography 39, 1349–1367.

Gordon, H.R., Wang, M., 1994. Influence of oceanic whitecaps on atmospheric correction of ocean-color sensors. Applied Optics 33, 7754–7763.

Gordon, H.R., Clark, D.K., Brown, J.W., Brown, O.B., Evans, R.H., Broenkow, W.W., 1983. Phytoplankton pigment concentrations in the Middle Atlantic Bight: comparison of ship determinations and CZCS estimates. Applied Optics 22, 20–36.

Gordon, H.R., Brown, O.B., Evans, R.H., Brown, J.W., Smith, R.C., Baker, K.S., Clark, D.K., 1988. A semianalytic radiance model of ocean color. Journal of Geophysical Research 93, 10,909–10,924.

Habas, E.J., Gilbert, C.K., 1974. The economic effects of the 1971 Florida red tide and the damage it presages for future occurrences. Environmental Letters 6, 139–147.

Hemmert, W.H., 1975. The public health implications of *Gymnodinium breve* red tides, A review of the literature and recent events. In: LoCicero, V.R. (Eds.), Proceedings of the First International Conference on Toxic Dinoflagellate Blooms, pp. 489–497.

Hoepffner, N., Sathyendranath, S., 1991. Effect of pigment composition on absorption properties of phytoplankton. Marine Ecology Progress Series 73, 11–23.

Holm-Hansen, O., Riemann, B., 1978. Chlorophyll a determination: improvements in methodology. Oikos 30, 438–447.

Hu, C., Carder, K.L., Muller-Karger, F.E., 2000. Atmospheric correction of SeaWiFS imagery over turbid coastal waters: a practical method. Remote Sensing of Environment 74, 195–206.

Hu, C., Muller-Karger, F.E., Biggs, D.C., Carder, K.L., Nababan, B., Nadeau, D., Vanderbloemen, J., 2003. Comparison of ship and satellite bio-optical measurements on the continental margin of the NE Gulf of Mexico. International Journal of Remote Sensing 24, 2597–2612.

Hu, C., Muller-Karger, F.E., Taylor, C., Carder, K.L., Kelble, C., Johns, E., Heil, C.A., 2005. Red tide detection and tracing using MODIS fluorescence data: a regional example in SW Florida coastal waters. Remote Sensing of Environment 97, 311–321.

IOCCG, 2006. Remote sensing of inherent optical properties: Fundamentals, tests of algorithms, and applications. In: Lee, Z.-P. (Ed.), Reports of the International Ocean-Colour Coordinating Group, No. 5, IOCCG, Dartmouth, Canada.

Kerfoot, J., Kirkpatrick, G., Lohrenz, S., Mahoney, K., Moline, M., Schofield, O., 2004. Vertical migration of *Karenia brevis* bloom: implications for remote sensing of harmful algal blooms. In: Steidinger, K.A., Landsberg, J.H., Tomas, C.R., Vargo, G.A. (Eds.), Harmful Algae 2002. Florida Fish and Wildlife Conservation Commission, Florida Institute of Oceanography, and Intergovernmental Oceanographic Commission of UNESCO, St. Petersburg, Florida, USA, pp. 279–181.

Kiefer, D., 1973. Fluorescence properties of natural phytoplankton populations. Marine Biology 22, 263–269.

Kiefer, D.A., SooHoo, J.B., 1982. Spectral absorption by marine particles of coastal waters of Baja California. Limnology and Oceanography 27, 492–499.

Kirkpatrick, G.J., Millie, D.F., Moline, M.A., Schofield, O., 2000. Optical discrimination of a phytoplankton species in natural mixed populations. Limnology and Oceanography 45, 467–471.

Kishino, M., Takahashi, M., Okami, N., Ichimura, S., 1985. Estimation of the spectral absorption coefficients of phytoplankton in the sea. Bulletin of Marine Science 37, 634–642.

Lambert, C.D., Bianchi, T.S., Santschi, P.H., 1999. Cross-shelf changes in phytoplankton community composition in the Gulf of Mexico (Texas shelf/slope): the use of plant pigments as biomarkers. Continental Shelf Research 19, 1–21.

Landsberg, J.H., Steidinger, K.A., 1998. A historical review of *Gymnodium breve* red tides implicated in mass mortalities of the manatee (*Trichechus manatus latiriostris*) in Florida, USA. In: Reguera, B., Blanco, J., Fernandez, M.L., Wyatt, T. (Eds.), Proceedings of the Eighth International Conference on Harmful Algal Blooms. Vigo, Spain, pp. 97–100.

Lee, Z., Carder, K.L., 2000. Band-ratio of spectral-curvature algorithms for satellite remote sensing? Applied Optics 39, 4377–4380.

Lee, Z., Carder, K.L., Hawes, S.K., Steward, R.G., Peacock, T.G., Davis, C.O., 1994. Model for the interpretation of hyperspectral remote-sensing reflectance. Applied Optics 33, 5721–5732.

Lee, Z., Carder, K.L., Mobley, C.D., Steward, R.G., Patch, J.S., 1999. Hyperspectral remote sensing for shallow waters: 2. Deriving bottom depths and water properties by optimization. Applied Optics 38, 3831–3843.

Lee, Z., Carder, K.L., Chen, R.F., Peacock, T.G., 2001. Properties of the water column and bottom derived from Airborne Visible Infrared Imaging Spectrometer (AVIRIS) data. Journal of Geophysical Research 106, 11,639–11,651.

Lee, Z.P., Carder, K.L., Steward, R.G., Peacock, T.G., Davis, C.O., Mueller, J.L., 1996. Remote-sensing reflectance and inherent optical properties of oceanic waters derived from above-water measurements. In: Ackleson, S.G., Frouin, R. (Eds.), Ocean Optics XIII. Proc. SPIE 2963, pp. 160–166.

Lee, Z.P., Carder, K.L., Mobley, C., Steward, R.G., Patch, J.S., 1998. Hyperspectral remote sensing for shallow waters: I. A semi-analytical model. Applied Optics 37, 6329–6338.

Lide, D.R., 1997. In: CRC Handbook of Chemistry and Physics. CRC Press, Boca Raton, Fla, pp. 4130–4136.

Lohrenz, S.E., Fahnenstiel, G.L., Kirkpatrick, G.J., Carroll, C.L., Kelly, K.A., 1999. Microphotometric assessment of spectral absorption and its potential application for characterization of harmful algal species. Journal of Phycology 35, 1438–1446.

Maffione, R.A., Dana, D.R., 1997. Instruments and methods for measuring the backward-scattering coefficient of ocean waters. Applied Optics 36, 6057–6067.

Mahoney, K.L., 2003. Backscattering of light by *Karenia brevis* and implications for optical detection and monitoring. Ph.D., University of Southern Mississippi, Stennis Space Center, 116pp.

Millie, D.F., Kirkpatrick, G.J., Vinyard, B.T., 1995. Relating photosynthetic pigments and in vivo optical density spectra to irradiance for the Florida red-tide dinoflagellate *Gymnodinium breve*. Marine Ecology Progress Series 120, 65–75.

Millie, D.F., Schofield, O.M., Kirkpatrick, G.J., Johnsen, G., Tester, P.A., Vinyard, B.T., 1997. Detection of harmful algal blooms using photopigments and absorption signatures: a case study of the Florida red tide dinoflagellate, *Gymnodinium breve*. Limnology and Oceanography 42, 1240–1251.

Mitchell, B.G., 1990. Algorithms for determining the absorption coefficient of aquatic particulates using the Quantitative Filter Technique (QFT). In: Spinrad, R.W. (Eds.), Ocean Optics X. Orlando, Florida, pp. 137–148.

Mobley, C.D., 1994. Light and Water: Radiative Transfer in Natural Waters. Academic Press, San Diego, 592pp.

Morel, A., 1974. Optical properties of pure water and pure sea water. In: Jerlov, N.G., Nielsen, E.S. (Eds.), Optical Aspects of Oceanography. Academic Press, London, pp. 1–24.

Morel, A., 1988. Optical modeling of the upper ocean in relation to its biogenous matter content (case I waters). Journal of Geophysical Research 93, 10,749–10,768.

Morel, A., Ahn, Y.-H., 1991. Optics of heterotrophic nanoflagellates and ciliates: a tentative assessment of their scattering role in oceanic waters compared to those of bacteria and algal cells. Journal of Marine Research 49, 177–202.

Morel, A., Bricaud, A., 1981. Theoretical results concerning light absorption in a discrete medium, and application to specific absorption of phytoplankton. Deep Sea Research 28, 1375–1393.

Morel, A., Prieur, L., 1977. Analysis of variations in ocean color. Limnology and Oceanography 22, 709–722.

Mueller, J.L., Fargion, G.S., 2002. Ocean optics protocols for satellite ocean color sensor validation, revision 3, volume 2. NASA/TM-2002-210004, NASA/GSFC, Greenbelt, Maryland, pp. 231–257.

Nelson, J.R., Guarda, S., 1995. Particulate and dissolved spectral absorption on the continental shelf of the southeastern United States. Journal of Geophysical Research 100, 8715–8732.

Nelson, N.B., Prezelin, B.B., Bidigare, R.R., 1993. Phytoplankton light absorption and the package effect in California coastal waters. Marine Ecology Progress Series 94, 217–227.

O'Reilly, J.E., Maritorena, S., Mitchell, B.G., Siegel, D.A., Carder, K.L., Garver, S.A., Kahru, M., McClain, C., 1998. Ocean color chlorophyll algorithms for SeaWiFS. Journal of Geophysical Research 103, 24,937–24,953.

Pope, R., Fry, E., 1997. Absorption spectrum (380–700 nm) of pure waters, II, Integrating cavity measurements. Applied Optics 36, 8710–8723.

Preisendorfer, R.W., 1961. Application of radiative transfer theory to light measurements in the sea. Monogr. 10, Paris, Intl. Union Geod. Geophys., pp. 11–30.

Qian, Y., Jochens, A.E., II, M.C.K., Biggs, D.C., 2003. Spatial and temporal variability of phytoplankton biomass and community structure over the continental margin of the northeast Gulf of Mexico based on pigment analysis. Continental Shelf Research 23, 1–17.

Roesler, C.S., Perry, M.J., Carder, K.L., 1989. Modeling in situ phytoplankton absorption from total absorption spectra in productive inland marine waters. Limnology and Oceanography 34, 1510–1523.

Schofield, O., Grzymski, J., Bissett, W.P., Kirkpatick, G.J., Millie, D.F., Moline, M., Roesler, C.S., 1999. Optical monitoring and forecasting systems for harmful algal blooms: possibility or pipe dream? Journal of Phycology 35, 1477–1496.

Schofield, O., Kerfoot, J., Mahoney, K., Moline, M., Oliver, M., Lohrenz, S., Kirkpatrick, G., 2006. Vertical migration of the toxic dinoflagellate *Karenia brevis* and the impact on ocean optical properties. Journal of Geophysical Research 111, C06009.

Shanley, E., Vargo, G.A., 1993. Cellular composition, growth, photosynthesis, and respiration rates of *Gymnodinium breve* under varying light levels. In: Smayda, T.J., Shimizu, Y. (Eds.), Toxic Phytoplankton Blooms in the Sea. Elsevier, New York, pp. 831–836.

Shuman, F.R., Lorenzen, C.J., 1975. Quantitative degradation of chlorophyll by a marine herbivore. Limnology and Oceanography 20, 580–586.

Siegel, D.A., Wang, M., Maritorena, S., Robinson, W., 2000. Atmospheric correction of satellite ocean color imagery: the black pixel assumption. Applied Optics 39, 3582–3591.

Smayda, T.J., 1997. Harmful algal blooms: their ecophysiology and general relevance to phytoplankton blooms in the sea. Limnology and Oceanography 42, 1137–1153.

Steidinger, K., 1975. Basic factors influencing red tides. In: LoCicero, V.R. (Eds.), Proceedings of the First International Conference on Toxic Dinoflagellate Blooms, pp. 153–162.

Steidinger, K.A., Haddad, K., 1981. Biologic and hydrographic aspects of red tides. BioScience 31, 814–819.

Steidinger, K.A., Vargo, G.A., Tester, P.A., Tomas, C.R., 1998. Bloom dynamics and physiology of *Gymnodinium breve*, with emphasis on the Gulf of Mexico. In: Anderson, E.M., Cembella, A.D., Hallengraff, G.M. (Eds.), Physiological Ecology of Harmful Algal Blooms. Springer, New York, pp. 135–153.

Stramski, D., Kiefer, D.A., 1991. Light scattering in microorganisms in the open ocean. Progress in Oceanography 28, 343–383.

Stuart, V., Sathyendranath, S., Platt, T., Maas, H., Irwin, B.D., 1998. Pigments and species composition of natural phytoplankton populations: effect on the absorption spectra. Journal of Plankton Research 20, 187–217.

Stumpf, R.P., Culver, M.E., Tester, P.A., Tomlinson, M., Kirkpatrick, G.J., Pederson, B.A., Truby, E., Ransibrahmanakul, V., Soracco, M., 2003. Monitoring *Karenia brevis* blooms in the Gulf of Mexico using satellite ocean color imagery and other data. Harmful Algae 2, 147–160.

Subramaniam, A., Carpenter, E.J., Falkowski, P.G., 1999. Bio-optical properties of the marine diazotrophic cyanobacteria *Trichodesmium spp.* II. A reflectance model for remote sensing. Limnology and Oceanography 44, 618–627.

Tester, P.A., Steidinger, K.A., 1997. *Gymnodinium breve* red tide blooms: initiation, transport, and consequences of surface circulation. Limnology and Oceanography 42, 1039–1051.

Tester, P.A., Stumpf, R.P., Vukovich, F.M., Fowler, P.K., Turner, J.T., 1991. An expatriate red tide bloom: transport, distribution, and persistence. Limnology and Oceanography 36, 1053–1061.

Tester, P.A., Stumpf, R.P., Steidinger, K., 1998. Ocean color imagery: What is the minimum detection level for *Gymnodinium breve* blooms? In: Reguera, B., Blanco, J., Fernandez, M.L., Wyatt, T. (Eds.), Harmful Algae. Xunta de Galacia and Intergovernmental Oceanographic Commission of UNESCO.

Tomlinson, M.C., Stumpf, R.P., Ransibrahmanakul, V., Truby, E.W., Kirkpatrick, G.J., Pederson, B.A., Vargo, G.A., Heil, C.A., 2004. Evaluation of the use of SeaWiFS imagery for detecting *Karenia brevis* harmful algal blooms in the eastern Gulf of Mexico. Remote Sensing of Environment 91, 293–303.

Trees, C.C., Clark, D.K., Bidigare, R.R., Ondrusek, M.E., Mueller, J.L., 2000. Accessory pigments versus chlorophyll a concentrations within the euphotic zone: a ubiquitous relationship. Limnology and Oceanography 45, 1130–1143.

Turner, J.T., Tester, P.A., 1997. Toxic marine phytoplankton, zooplankton grazers, and pelagic food webs. Limnology and Oceanography 42, 1203–1214.

Twardowski, M.S., Boss, E., Macdonald, J.B., Pegau, W.S., Barnard, A.H., Zaneveld, J.R.V., 2001. A model for estimating bulk refractive index from the optical backscattering ratio and the implications for understanding particle composition in case I and case II waters. Journal of Geophysical Research 106, 14,129–14,142.

Ulloa, O., Sathyendranath, S., Platt, T., 1994. Effect of the particle-size distribution on the backscattering ratio in seawater. Applied Optics 33, 7070–7077.

Vargo, G.A., Carder, K.L., Gregg, W., Shanley, E., Heil, C., Steidinger, K.A., Haddad, K.D., 1987. The potential contribution of primary production by red tides to the west Florida shelf ecosystem. Limnology and Oceanography 32, 762–767.

Vargo, G.A., Heil, C.A., Spence, D., Neely, M.B., Merkt, R., Lester, K., Weisberg, R.H., Walsh, J.J., Fanning, K., 2001. The hydrographic regime, nutrient requirements, and transport of a *Gymnodinium breve* Davis red tide on the West Florida Shelf. In: Hallegraff, G.M., Blackburn, S.I., Bolch, C.J., Lewis, R.J. (Eds.), Proceedings of the Ninth International Conference on Harmful Algae, 11–15 February, 2000, Hobart, Australia, pp. 157–160.

Vodacek, A., Blough, N.V., 1997. Seasonal variation of CDOM and DOC in the Middle Atlantic Bight: terrestrial inputs and photooxidation. Limnology and Oceanography 42, 674–686.

Walsh, J.J., Steidinger, K.A., 2001. Saharan dust and Florida red tides: the cyanophyte connection. Journals of Geophysical Research 106, 11,597–11,612.

Wright, S.W., Jeffrey, S.W., Mantoura, R.F.C., Llewellyn, C.A., Bjornland, T., Repeta, D., Welschmeyer, N., 1991. Improved HPLC method for the analysis of chlorophylls and carotenoids from marine phytoplankton. Marine Ecology Progress Series 77, 183–196.

Yentsch, C.S., 1962. Measurement of visible light absorption by particulate matter in the ocean. Limnology and Oceanography 7, 207–217.